Synchrotron Studies of an X-ray Transmission Grating

by

Christie S. Nelson

Submitted to the Department of Physics
in partial fulfillment of the requirements for the degree of

Bachelor of Science in Physics

at the

MASSACHUSETTS INSTITUTE OF TECHNOLOGY

May 1994

© Massachusetts Institute of Technology 1994. All rights reserved.

Author .....
Department of Physics
May 6, 1994

Certified by .....
Claude R. Canizares
Professor of Physics
Thesis Supervisor

Accepted by .....
Aron M. Bernstein
Chairman, Undergraduate Thesis Committee

Synchrotron Studies of an X-ray Transmission Grating

by

Christie S. Nelson

Submitted to the Department of Physics
on May 6, 1994, in partial fulfillment of the
requirements for the degree of
Bachelor of Science in Physics

Abstract

Transmission gratings designed for use in the High Energy Transmission Grating Spectrometer (HETGS) of the Advanced X-ray Astrophysics Facility are composed of gold bars with periods of 0.2 and 0.4 μm. These gratings are designed to optimize both the spectral resolution and instrumental efficiency over the HETGS operating energy range of 0.4–8 keV. On the grating facet level, the most significant factor determining the spectral resolution is period variation (Canizares *et al.*, 1992), which can be measured by studying high grating diffraction orders. Grating facet efficiency can be calculated from theory using knowledge of grating parameters such as the bar height, bar width to period ratio, and bar shape. But since precise knowledge of these parameters is difficult to obtain, grating facet efficiency should be experimentally verified. In this thesis, I describe measurements of grating facet period variation and efficiency that were performed using synchrotron radiation at the Daresbury Laboratory, Synchrotron Radiation Source and the Brookhaven National Laboratory, National Synchrotron Light Source. A 3σ upper limit on period variation at an energy of 8.442 keV is measured as 1.8E-4, and suggestions for further studies are made based on the results of the Daresbury tests. Efficiency results from Brookhaven show good agreement between the measured efficiencies and the predicted grating efficiencies for much of the 0.7–6.6 keV energy range studied. However, there is significant deviation between the theoretical model and the data in the energy range of 1.5–2 keV. In this thesis, I show that variation of model parameters is ineffective at eliminating the deviation in this energy range. Possible explanations for this discrepancy as well as future efficiency test plans are discussed.

Thesis Supervisor: Claude R. Canizares
Title: Professor of Physics

Synchrotron Studies of an X-ray Transmission Grating

by

Christie S. Nelson

Submitted to the Department of Physics
on May 6, 1994, in partial fulfillment of the
requirements for the degree of
Bachelor of Science in Physics

Abstract

Transmission gratings designed for use in the High Energy Transmission Grating Spectrometer (HETGS) of the Advanced X-ray Astrophysics Facility are composed of gold bars with periods of 0.2 and 0.4 μm. These gratings are designed to optimize both the spectral resolution and instrumental efficiency over the HETGS operating energy range of 0.4–8 keV. On the grating facet level, the most significant factor determining the spectral resolution is period variation (Canizares *et al.*, 1992), which can be measured by studying high grating diffraction orders. Grating facet efficiency can be calculated from theory using knowledge of grating parameters such as the bar height, bar width to period ratio, and bar shape. But since precise knowledge of these parameters is difficult to obtain, grating facet efficiency should be experimentally verified. In this thesis, I describe measurements of grating facet period variation and efficiency that were performed using synchrotron radiation at the Daresbury Laboratory, Synchrotron Radiation Source and the Brookhaven National Laboratory, National Synchrotron Light Source. A 3σ upper limit on period variation at an energy of 8.442 keV is measured as 1.8E-4, and suggestions for further studies are made based on the results of the Daresbury tests. Efficiency results from Brookhaven show good agreement between the measured efficiencies and the predicted grating efficiencies for much of the 0.7–6.6 keV energy range studied. However, there is significant deviation between the theoretical model and the data in the energy range of 1.5–2 keV. In this thesis, I show that variation of model parameters is ineffective at eliminating the deviation in this energy range. Possible explanations for this discrepancy as well as future efficiency test plans are discussed.

Thesis Supervisor: Claude R. Canizares
Title: Professor of Physics

Acknowledgments

I would like to thank my advisor Claude Canizares for his time, guidance, and suggestions and for the responsibility he has given me over the last year. I would like to thank Tom Markert for the past three and a half years that I have been able to work with him. Tom has given me many opportunities to pursue exciting projects and with his patience, enthusiasm, and knowledge, he has taught me much of what I will take away from my four years at MIT. It would be impossible for me to say enough about what Tom has done for me, so I would just like to say thank you, Tom, once again.

The NSLS tests were largely made possible by Dale Graessle. I would like to thank him for the use of the reflectometer chamber and its contents, for his generosity with his time and experience, and for his patience with our many questions and requests. I would also like to acknowledge the help of Richard Blake for his advice on our tests, Dave Breslau for designing and making the grating and slit holder modifications, Russ Ingram for designing and building the reflectometer chamber, Don Humphries for providing detector slits, Mike Sagurton for help at the beam line, and Tom Burbine for help with collecting the data.

I would like to thank Salim Abdali and Finn Christensen for organizing the Daresbury tests, giving us some of their beam time and the use of their equipment, and helping me out via e-mail with my many questions. Also, thanks to Allan Hornstrup, Peter Frederiksen, and Konstantin Borozdin for their time spent at Daresbury on our experiment. I would also like to thank my Daresbury "chaperone"— Kathy Flanagan— for her contributions both at Daresbury and at the NSLS. Her experience, in every sense of the word, has been extremely helpful to me over the last year and I really appreciate her friendship.

Dan Dewey and Mark Schattenburg have been very helpful with their many suggestions. Dan's experience with testing gratings and the diagnostic tests that he carried out on grating HX101 allowed us to plan the NSLS tests and Mark's program XRAY has been our primary means of modelling grating performance. I would like

to thank the two of them as well as Rich Aucoin, Chris Pak, Mike McGuirk, and the rest of the HETG group for suggestions ranging from analyzing data to refining the synchrotron test procedures.

For the last two semesters, I have had the help of fellow UROP student Yun Song. I would like to thank him for his work on the IDL program and the vector theory, his help with the data analysis, and his company on those long nights of data runs at the NSLS. I also appreciate the help given by former UROP'er and present-day graduate student James (Gerbs) Bauer on the NSLS nights in both July and January. Thanks also to the many students— Una Hwang, Bob Rutledge, Dave Buote, Eric Gaidos, Rich Lester, Vicki Scheribel— who reside on the 6th floor of the CSR and are always ready to tackle my UNIX, C, LaTeX, etc. questions.

Finally, I would like to thank my family— Grandma, Mom, Kent, Brant, Kelly, Matthew, and Jake— and my support network here at MIT— Manish, Amy, and Vivian— for encouraging me throughout my years here.

Contents

1 Introduction **11**

1.1 Cosmic X-ray Spectroscopy 11

1.2 The HETGS on AXAF 13

1.3 HETGS Performance and Calibration Plans 19

2 Synchrotron Studies of X-ray Transmission Gratings **21**

2.1 Usefulness of Synchrotrons 21

2.2 Measurements of Resolving Power 24

2.3 Measurements of Efficiency 27

3 Measurements of Resolving Power at the Daresbury Laboratory Synchrotron Radiation Source **30**

3.1 Goal of Tests 30

3.2 Test Procedure 31

3.3 Summary of Data 36

3.4 Conclusions 41

4 Measurements of Efficiency at the National Synchrotron Light Source **45**

4.1 Goal of Tests 45

4.2 Test History 47

4.3 Test Set-up 49

4.4 January 1994 Preliminary Tests 51

4.4.1 Verifying Test Configuration 51

4.4.2 Detector Cross-Calibration 51

4.5 Efficiency Test Results 57

5 Understanding the National Synchrotron Light Source Results 66

5.1 Theoretical Model with Standard Parameters vs. Data 66

5.2 Parameter Variation 69

5.3 Conclusions on Theory/Data Discrepancy 77

6 Conclusions on the National Synchrotron Light Source Tests 80

6.1 Progress Toward Goals 80

6.2 Future Plans 82

6.2.1 HX101 re-testing 83

6.2.2 flight-like HEG testing 84

6.2.3 MEG testing 86

A Efficiencies of HX101 in the energy range of 0.708–6.6 keV 88

List of Figures

1-1 A schematic of the Advanced X-ray Astrophysics Facility. 12

1-2 McKenzie *et al.*, 1980, figure of solar flare spectrum. 14

1-3 The AXAF High Energy Transmission Grating Spectrometer. 15

1-4 The AXAF High Energy Transmission Grating. 17

1-5 Schematic of an HEG grating in the HETGS. The thin plating base is not shown. 18

1-6 SEM picture of a section of HETGS grating HX101. 19

2-1 Schematic diagram of the plans for the x-ray ring of the National Synchrotron Light Source (Kunz *et al.*, 1979). 23

2-2 Schematic diagram of a cross-section of a small section of a grating. Relevant grating parameters are labeled. 26

2-3 Example of gold transmission grating efficiency over entire HETGS energy range, calculated using XRAY. Period of grating is 2000 Å, bar height is 4000 Å, and grating bar thickness is 1000 Å. 29

3-1 Schematic of test set-up at the Synchrotron Radiation Source. 32

3-2 HX101 illuminated strips for the twelfth grating diffraction order measurements. 35

3-3 Rocking curve of zeroth grating diffraction order. Each data point is for a ∼2 second collection at each analyzer crystal position. The solid line is the best Gaussian fit to the data. One motor step is equal to 0.05 arcsec. 37

3-4 Rocking curve of twelfth grating diffraction order at the #6 grating position (see Figure 3-2). Each data point is for a ~20 second collection at each analyzer crystal position. The solid line is the best Gaussian fit to the data. One motor step is equal to 0.05 arcsec. 38
3-5 FWHM's of twelfth grating diffraction orders for the 21 grating strips as defined by Figure 3-2. 42
3-6 Contour plot of the period variation of test grating HX101 as measured by Dan Dewey at the MIT laser reflection facility. 44

4-1 Floor plan of the National Synchrotron Light Source. 46
4-2 July 1993, first order efficiency measurements. 48
4-3 Test set-up at downstream section of beam line X8A. 50
4-4 2.03–4.2 keV slitted detector and monitor detector calibration results. 53
4-5 0.708–2.025 keV slitted detector and monitor detector calibration results. 54
4-6 2.83–6.5 keV slitted detector and monitor detector calibration results. The detector cross-calibration scans were actually conducted in 5 and 10 motor step intervals of the slitted detector. Because all efficiency tests were conducted in 40 motor step intervals, the calculated ratios were normalized by dividing by 8 or 4 in order for the ratios to approach unity and also to facilitate easier comparison with Figure 4-4 and 4-5. 55
4-7 2 mil slitted detector scan at 1.417 keV. Zeroth grating diffraction order on left and first grating diffraction order on right. 58
4-8 8 mil slitted detector scan at 2.5 keV. Zeroth grating diffraction order on left and first grating diffraction order on right. 59
4-9 2 mil slitted detector scan at 5.6 keV. Zeroth grating diffraction order on left and first grating diffraction order on right. 60
4-10 2 mil slitted detector scan at 4.4 keV along with limits used for calculating zeroth and first order efficiency (vertical lines). Zeroth grating diffraction order on left and first grating diffraction order on right. . . 62
4-11 Zeroth order efficiency. 64

4-12 First order efficiency. 65

5-1 Theoretical and measured first order efficiencies. The theoretical efficiencies were calculated using XRAY. 68

5-2 Effect of variation in the thickness of the gold in the plating base. The upper solid line corresponds to a 180 Å layer and the lower dashed line corresponds to a 220 Å layer. 71

5-3 Fractional difference between efficiencies calculated using a rectangular bar shape and a trapezoidal bar shape. The dimensions of the trapezoid are such that the trapezoid and the rectangle have equal areas. The difference plotted is the rectangular efficiency minus the trapezoidal efficiency divided by the rectangular efficiency, as a function of energy. 73

5-4 Effect of variation of the grating bar width to period ratio parameters on first order efficiency. The upper solid line corresponds to the nominal value minus σ and the lower dashed line corresponds to the nominal value plus σ. 75

5-5 The best-fit theoretical model to the efficiency data. The parameters used by XRAY to create the model are listed in Table 5-2. 76

5-6 Scalar theory vs. vector theory for HX101 efficiency. The solid line corresponds to the scalar theory and the dashed line corresponds to the vector theory. 78

6-1 Theoretical first order efficiency for a flight-like HEG grating. Parameters used by XRAY include period 2000 Å, bar height 6000 Å, bar width 1000 Å, polyimide thickness 1 μm, and standard thicknesses for plating base materials. 85

6-2 Theoretical first order efficiency for an MEG grating. Parameters used by XRAY include period 4000 Å, bar height 4000 Å, bar width 2000 Å, polyimide thickness 5000 Å, and standard thicknesses for plating base materials. 87

List of Tables

3.1 HX101 parameters as measured at MIT (Dewey, 1993)(Abdali *et al.*, 1993). 33

3.2 FWHM data of direct beam and zeroth and twelfth grating diffraction orders. The illuminated part of grating is taken from Figure 3-2. . . . 39

3.3 $\Delta p/p$ components. 40

4.1 Equipment and number of tests planned for efficiency measurements. 57

5.1 Plating base material and support structure thicknesses used for calculating the theoretical efficiencies (Schattenburg, 1994, private communication). 67

5.2 Parameters used by XRAY to create the best-fit theoretical model to the efficiency data. 77

A.1 HX101 zeroth and first order efficiencies, as measured at the National Synchrotron Light Source in January 1994. 89

Chapter 1

Introduction

The Advanced X-ray Astrophysics Facility (AXAF)— planned for launch in 1998— is the x-ray element in NASA's Great Observatories Program. AXAF is comprised of a telescope (the High Resolution Mirror Assembly) and scientific instruments designed to study cosmic x-ray sources. The science instruments are the High Resolution Camera, a CCD imaging detector, and both Low and High Energy Transmission Grating Spectrometers. A drawing of a recent design of the satellite is shown below in Figure 1-1.

The High Energy Transmission Grating Spectrometer (HETGS) is being built at MIT under the direction of Professor Claude Canizares. The testing of components of this instrument, which involved the use of synchrotron radiation, is the subject of this thesis.

1.1 Cosmic X-ray Spectroscopy

Transmission gratings were first used for x-ray astrophysics on a rocket flight in 1968 in which a solar flare was observed (Vaiana *et al.*, 1968). Since then, other astrophysical spectra that have been observed with the transmission gratings of the Einstein Observatory— see Canizares and Kruper, 1984— and the European x-ray satellite EXOSAT— see Paerels *et al.*, 1986, and Paerels *et al.*, 1988— have demonstrated the potential of transmission grating technology for the field of astrophysics. Further-

Figure 1-1: A schematic of the Advanced X-ray Astrophysics Facility.

more, due to advances in the fabrication processes of sub-micron structures, AXAF's transmission gratings in the HETGS promise higher spectral resolving powers and diffraction efficiencies than these early x-ray satellites (Schattenburg *et al.*, 1988).

It is important to maximize the spectral resolving power of an x-ray transmission grating in order to optimize the study of astrophysical objects. Cosmic plasmas with temperatures on the order of tens of millions of degrees K are rich in x-ray emission lines, many of which are quite closely spaced and therefore require maximal spectral resolving power from the instruments that are used to study them. Such cosmic plasmas are associated with some of the more interesting astrophysical objects—quasars, supernovae and supernova remnants, clusters of galaxies, stellar coronae, and compact objects such as neutron stars and black holes. For an example of the multitude of closely spaced x-ray emission lines, see Figure 1-2 (McKenzie *et al.*, 1980) below for an x-ray spectrum of the sun taken with a crystal spectrometer. In addition to measuring the strengths of closely-spaced spectral lines, high spectral resolution also permits the measurement of Doppler velocities, such as the bulk velocity of exploding stars and the orbital motion of binary star systems.

High efficiency is important for x-ray transmission grating spectrometers due to the weakness of many cosmic x-ray sources. Since the flux from an x-ray source of given luminosity decreases quadratically with distance, high efficiency is especially important for the study of extra-galactic x-ray sources.

1.2 The HETGS on AXAF

The HETGS (shown below in Figure 1-3) includes the High Resolution Mirror Assembly (HRMA), an array of 336 transmission grating facets (each $\sim$1 inch square), and an imaging detector. The array of grating facets (HETG) can be moved into the path of the x-rays in order to disperse the x-rays across the focal plane of the telescope. The x-rays can then be detected by either the AXAF CCD Imaging Spectrometer or the High Resolution Camera.

The operating energy range of the HETGS is 0.4–8 keV with resolving powers

Figure 1-2: McKenzie *et al.*, 1980, figure of solar flare spectrum.

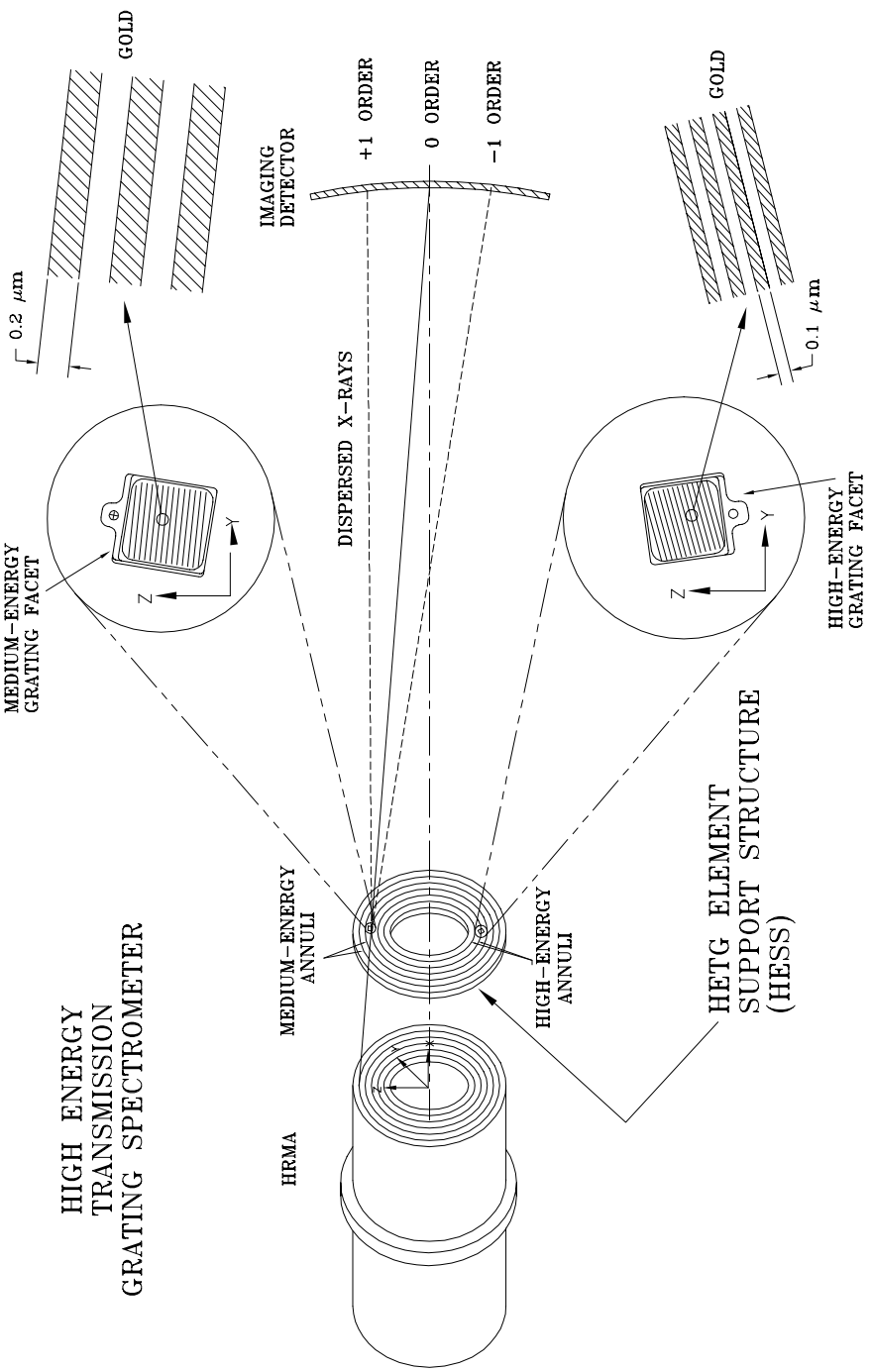

Figure 1-3: The AXAF High Energy Transmission Grating Spectrometer.

of 100–1000. In order to optimize the HETGS performance over this entire energy range, grating facets with two different periods— 2000 Å with 7000 Å high grating bars (high energy gratings, or HEG) and 4000 Å with 4000 Å high grating bars (medium energy gratings, or MEG)— are included in the array. These gratings use the phase shifting property of the grating bars to maximize instrumental efficiency. That is, if the x-rays that pass through the bars experience a phase shift of $\sim \pi$ and interfere with the x-rays that pass through the empty space between bars, the undiffracted beam (zeroth order) is decreased in intensity and there is an increase in the intensity of some of the higher orders. The bar thickness can be chosen to increase the efficiency— i.e. the intensity in the first order— of the grating. The thickness of the HEG bars are chosen to optimize the efficiency at higher energies and the MEG bars are chosen to optimize the efficiency at lower energies in the HETGS operating energy range.

The array of HEG and MEG gratings in the HETGS is shown below in Figure 1-4. The HEG's will be located in the inner ring of the array and the MEG's will be in the outer ring. This arrangement takes advantage of the fact that the inner part of the telescope is more efficient for the reflection of higher energy radiation.

The individual grating facets of the HETGS are fabricated using holography techniques. The first step in this process is the exposure of a layer of photo-resist to converging UV laser beams, which produce a periodic pattern in the photo-resist. This layer of photo-resist is the top layer of a structure that consists of layers of SiO_2, anti-reflection coating, plating base materials such as gold and chromium, and polyimide (the eventual support structure of the grating) all on top of a silicon wafer.

After the photo-resist is developed, first the exposed SiO_2 and then the anti-reflection coating layers are removed with reactive ion etchers. The remaining structure is then electro-plated with gold and a reactive ion etcher is used to remove the anti-reflection coating between the gold grating bars. Finally, the silicon wafer is removed using a chemical etching process and the remaining structure is the $\sim$0.7 μm (for HEG's) high gold grating bars on the thin ($\leq$ few hundred Å), plating base materials and the $\sim$1 μm thick polyimide layer. A schematic side view of an HEG

Figure 1-4: The AXAF High Energy Transmission Grating.

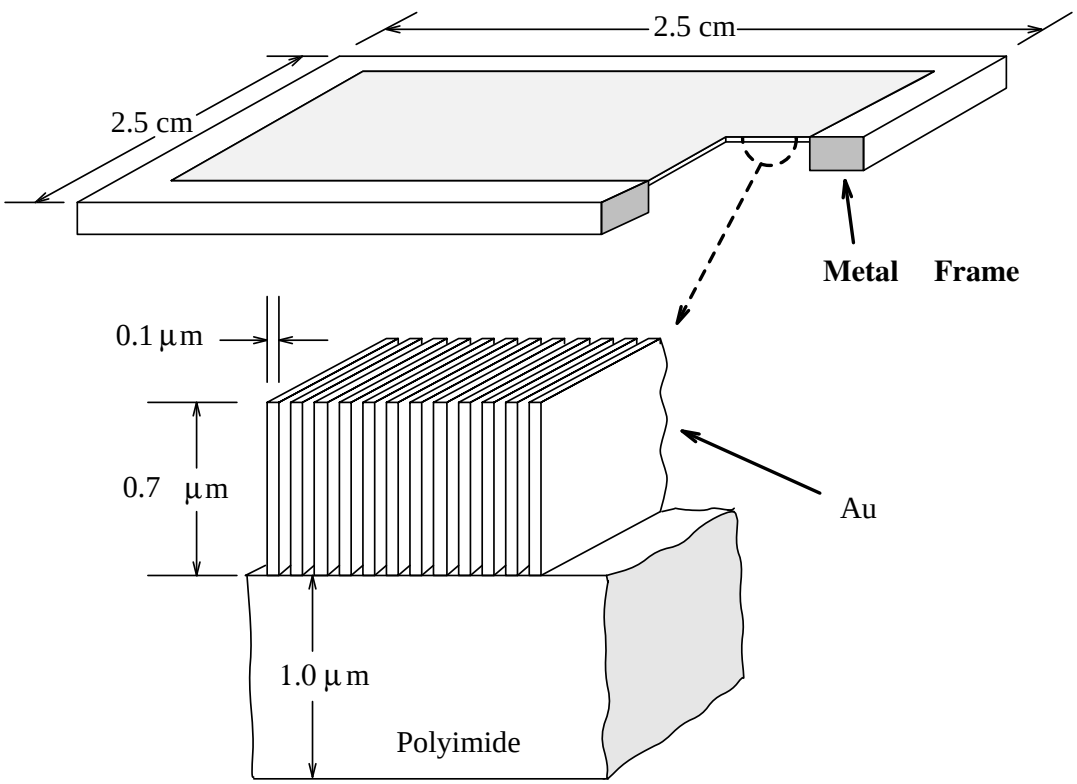

Figure 1-5: Schematic of an HEG grating in the HETGS. The thin plating base is not shown.

grating is shown in Figure 1-5 and in Figure 1-6, an electron microscope picture of part of the grating facet that was studied in the tests described in this thesis (HX101) is shown.

Figure 1-6: SEM picture of a section of HETGS grating HX101.

1.3 HETGS Performance and Calibration Plans

Two of the most important properties of instruments in cosmic x-ray spectroscopy— as explained in Section 1.1— are high spectral resolution and high efficiency. For the HETGS, the instrument specification for spectral resolution ($E/\Delta E$) is that it should peak at $\sim$1000. The instrument specification for efficiency is an efficiency greater than 10% for energies greater than 1 keV (*AXAF-I Level I Program Requirements Document*), where the relevant efficiency is defined as the ratio of the flux going into the first diffraction orders to the flux incident on the grating.

Some of the components that reduce the spectral resolution of the HETGS are the HRMA spatial resolution (the blur), imaging detector spatial resolution, grating period variation across the HETG, and grating period variation within individual gratings. So, on the level of individual grating facets, the component of spectral

resolution to be minimized is period variation. For individual facets of the HETG, the period variation ($\Delta p/p$) is required to be less than 1.8E-4 rms (Markert, 1994, private communication).

The period variation of HETGS grating facets are routinely measured at MIT using reflection of a laser (UV for HEG's and optical for MEG's) off of the grating facets. Though this method is convenient to use, it does not measure the real parameter of interest— period variation for *transmitted* x-rays. For grating facet calibration purposes, it is assumed that the period variation for laser reflection and x-ray transmission are equivalent. A test of the validity of this assumption is detailed in Chapter 3.

High instrumental efficiency is important in cosmic x-ray spectroscopy due to the weakness of many x-ray sources in space. As was mentioned earlier, the efficiency of transmission gratings can be maximized for an energy range by using the phase shifting property of the grating bars. For the purposes of cosmic x-ray spectroscopy, though, high grating efficiency is not enough— the efficiency also needs to be well known. The instrumental goal as of this writing is to know the efficiency of the array of gratings in the HETGS to 3%.

In order to verify the required efficiency, a 17 meter long facility is currently being built at MIT for the efficiency calibration of HETGS grating facets. This facility consists of a multi-anode x-ray source, a focusing optic, and a flow proportional counter. Grating efficiency will be measured in this facility at several different line energies. This facility will also allow for the limits on grating spectral resolution (up to $E/\Delta E < 800$) to be determined.

For efficiency measurements at the MIT facility, there are plans to use calibration transfer standards, which would be gratings that have well characterized efficiencies over the entire HETGS energy range. The efficiencies would be measured at a synchrotron source (much as described in Chapter 4 of this thesis) and then the transfer standards would be used in the MIT facility to verify consistency in the testing process.

Chapter 2

Synchrotron Studies of X-ray Transmission Gratings

Synchrotron sources have two very useful properties for grating studies of the type described in this thesis. Those two properties are high intensity and a broad spectral range of continuum radiation. High intensity is useful for the study of high grating diffraction orders, which is necessary for measurements of grating resolving power (as will be explained in Section 2.2). High intensity also allows any measurement to be made relatively quickly. The broad spectral range of the continuum radiation is useful for in-depth grating efficiency measurements as testing can cover a wide energy range at discrete energies, which are not limited to atomic line energies.

2.1 Usefulness of Synchrotrons

In a synchrotron, particles are maintained in a circular orbit due to the presence of magnetic fields set up by an array of bending magnets. For high energy synchrotrons, the particles are initially accelerated with the use of a linear accelerator and then are injected into a circular vacuum chamber. Within the evacuated ring, phased RF cavities are used to accelerate the particles (Hughes, 1991). The particles themselves are bunched within the ring and several bunches of particles may be in the ring at a given time. The particles accelerated in synchrotrons are either protons or electrons.

For the tests discussed in this thesis, electron synchrotrons were used. An example from Kunz *et al.*, 1979, of the equipment in a typical synchrotron storage ring— Brookhaven National Laboratory's National Synchrotron Light Source— is shown in Figure 2-1. Note that Figure 2-1 is the plan for the National Synchrotron Light Source before it was built and that the actual design of the facility is somewhat different.

Since an accelerated charged particle emits radiation, electrons in a synchrotron emit radiation consisting of a fundamental frequency— associated with the frequency of revolution— as well as smeared out harmonics of this fundamental frequency. Some of the properties of this radiation are its continuous spectrum from infrared to x-ray, short (on the order of picoseconds) pulse lengths, and collimation into a narrow cone since the radiation is emitted in the instantaneous direction of motion (because the velocity of the electrons is $\sim$c). The main advantage of synchrotron radiation over other continuous spectrum x-ray sources— such as rotating anode sources in which about half of the emitted radiation is continuum— is its higher intensity (Kunz *et al.*, 1979).

Synchrotron radiation is useful for experiments once it exits the storage ring through a beam port. The beam then travels through a beam line, which can be equipped with a variety of optics, monochromators, and detectors. What will follow is a discussion of typical beam line equipment used for x-ray experiments.

A common beam line optic useful for focusing the beam is the mirror. Some of the requirements that the mirror must meet are a small rms surface roughness (in order to limit scattering), large physical size due to the small grazing incidence angles often required, high reflectivity for the relevant spectral range, and the ability to stand up to high power densities. The first two of these requirements are directly opposed to each other since larger mirrors tend to have larger rms surface roughness. The third requirement— high reflectivity— is often met with the use of mirror coatings (Kunz *et al.*, 1979). The final requirement makes the use of some sort of cooling device necessary.

Other types of beam line optics include gratings (reflection, (a)spherical concave, transmission, holographic), Fresnel zone plates, and crystals (used as monochroma-

Figure 2-1: Schematic diagram of the plans for the x-ray ring of the National Synchrotron Light Source (Kunz *et al.*, 1979).

tors). For crystals, the desired crystal resolution must be chosen in order to optimize two effects— high resolution crystals cause a reduction in beam intensity while low resolution crystals cause an increase in the divergence of the beam.

The most common type of monochromator used for x-ray studies is the crystal pair. Two flat crystals in a parallel arrangement are useful in that they maintain the direction of the beam while causing it only a parallel displacement. For beam focusing purposes, bent crystals are sometimes used as monochromators.

An additional use of double crystal monochromators is to eliminate high order harmonics, which are seldom desired. This elimination can be accomplished by using crystals of different types and de-tuning the first crystal. The second crystal then diffracts only the fundamental frequency and not the high order harmonics (Kunz *et al.*, 1979). Harmonic elimination can also be accomplished with the use of filters.

There is a wide range of detectors suitable for synchrotron studies. The most demanding requirement placed on these detectors is that they must have the capacity to withstand— and remain linear when exposed to— high count rates. When energy resolution is necessary, useful detectors include proportional counters, scintillation counters, and semiconductor counters. For imaging purposes, multi-wire proportional counters, linear solid state detectors, and cameras with fluorescent screens are often used.

2.2 Measurements of Resolving Power

As was discussed earlier (Section 1.3), period variation is the major factor governing the spectral resolution of a grating. This variation can be determined by measuring the width of the diffraction orders. To see this, a look at the equation governing diffraction— the so-called "grating equation"— is required.

For the cross-section of a grating shown below in Figure 2-2, the grating equation,

$$m\lambda = psin\theta, \tag{2.1}$$

holds in the Fraunhofer diffraction limit (i.e. when all grating features are assumed to

be much larger than the wavelength of incident radiation), where m is the diffraction order, λ is the wavelength of incident radiation, p is the period of the grating, and θ is the angular dispersion (Born and Wolf, 1970). Using the above equation, the two components of the angular width of the orders ($\Delta\theta$ = full width at half maximum of the diffracted line)— one due to the bandwidth of the x-ray source (e.g. the natural line width for an electron bombardment target) and the other to the grating period variation— can be derived. These two contributions are shown below in equations 2.2 and 2.3:

$$\Delta\theta_m^{\lambda} = tan(\theta_m)\frac{\Delta\lambda}{\lambda} \tag{2.2}$$

$$\Delta\theta_m^{p} = tan(\theta_m)\frac{\Delta p}{p} \tag{2.3}$$

When a synchrotron source is used with monochromator crystals to set the energy, the bandwidth arises from the rocking curve widths of the monochromator crystals. These $\Delta\theta$ components add in quadrature to give the total $\Delta\theta$ for the mth order as shown in the following (Abdali *et al.*, 1993):

$$(\Delta\theta_m)^2 = (\Delta\theta_m^{\lambda})^2 + (\Delta\theta_m^{p})^2 \tag{2.4}$$

From the above equation, it can be seen that an independent measurement of $\Delta\theta_m^{\lambda}$ can be used with a measurement of $\Delta\theta_m$ to obtain the period variation ($\frac{\Delta p}{p}$). The following is a final equation showing this relation:

$$\frac{\Delta p}{p} = \frac{1}{tan\theta_m}\sqrt{(\Delta\theta_m)^2 - (\Delta\theta_m^{\lambda})^2} \tag{2.5}$$

In practice, measurements of the period variation are often difficult to make because the contribution to the width of the grating diffraction orders from additional crystals (crystals used for grating order, selection purposes after the x-rays have passed through the grating) is so large. In order to make the contribution from the period variation comparable in size to this additional crystal component, high grating diffraction orders must be studied. (As a result of the $tan(\theta_m)$, which is large for large

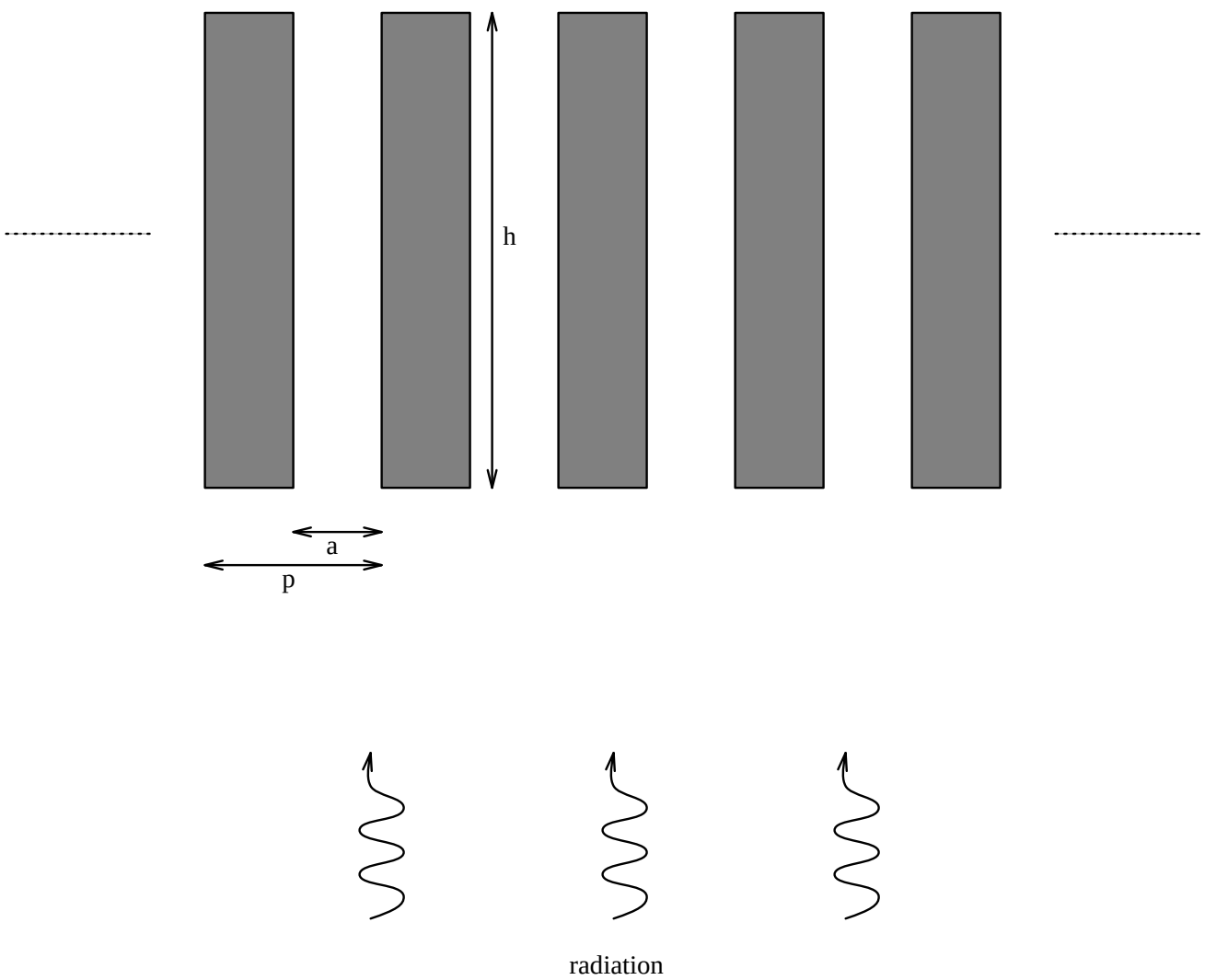

Figure 2-2: Schematic diagram of a cross-section of a small section of a grating. Relevant grating parameters are labeled.

m, $\Delta\theta_m^p$ becomes significant [equation 2.3].) Of course, higher grating diffraction orders also mean a larger component to $\Delta\theta_m$ from the monochromator crystals. This does not present a problem as long as $\frac{\Delta\lambda}{\lambda}$ is less than or approximately equal to $\frac{\Delta p}{p}$. In Chapter 3 we discuss measurements of resolving power made for a sample HEG grating.

2.3 Measurements of Efficiency

The advantage of using phased gratings— as opposed to opaque gratings— for cosmic x-ray spectroscopy is the higher efficiency that can be obtained (at some energies) due to the phase shifting property of phased gratings. When the bar height, h (see Figure 2-2), is made to satisfy the condition that the phase shift, $\Delta\phi$, is equal to π, destructive interference occurs and the zeroth grating diffraction order disappears. Since the total light must be conserved, the first grating diffraction orders are increased in intensity.

For a given phased grating with bar height h, the phase shift matching condition can only be satisfied at a single wavelength. But at wavelengths near this one particular wavelength, partial destructive interference of the zeroth grating diffraction order occurs and the first grating diffraction orders are enhanced. The result is a range of wavelengths for which the grating efficiency is maximized.

For a quantitative look at the higher efficiency of phased gratings compared to opaque gratings, equations 2.6 and 2.7 below show the grating efficiencies as functions of the grating parameters in Figure 2-2 (Schattenburg *et al.*, 1988):

$$\eta_{opaque} = 2 \times \frac{sin^2(\frac{\pi a}{p})}{\pi^2} \tag{2.6}$$

$$\eta_{phased} = \eta_{opaque} \times [1 + e^{-2kh\beta} - 2e^{-kh\beta}cos(kh\delta)] \tag{2.7}$$

where k is the wavenumber $(2\pi/\lambda)$ of incident light, β is the imaginary part of the index of refraction, δ is the real part of the index of refraction, and η is the efficiency in the combined (+ and −) first orders. When absorption is ignored (the fully-phased case), equation 2.7 reduces to the following (Schattenburg *et al.*, 1988):

$$\eta_{fully-phased} = 8 \times sin^2(\frac{kh\delta}{2}) \times \frac{sin^2(\frac{\pi a}{p})}{\pi^2} \tag{2.8}$$

From equation 2.8, it can be seen that at an optimal wavelength ($\lambda = 2h\delta$), the fully-phased grating efficiency is four times the opaque grating efficiency[1].

An example of the efficiency of a gold transmission grating (period 2000 Å, bar height 4000 Å, and grating bar thickness 1000 Å) over the HETGS energy range is shown below in Figure 2-3. The efficiencies were calculated for this figure using Schattenburg's program XRAY. In the figure, the peak at ~1600 eV is due to the phase shift matching of the x-rays through the 4000 Å thick gold bars. The four[2] dips in the efficiency in the 2000–3500 eV range are due to the M edges of the gold, where the grating absorbs more of the incident radiation. The steady decline in efficiency at energies of 4000 eV and higher is a result of the gold becoming transparent to the x-rays, which causes an increase in the zeroth grating diffraction order and a compensating decrease in the first grating diffraction orders.

The measurement of transmission grating efficiency is a straightforward procedure involving the simultaneous measurement of the intensity of light (i.e., x-rays) incident on the grating and the intensity of light in both, first grating diffraction orders[3]. The use of synchrotron radiation allows for many efficiency measurements to be made over the entire HETGS energy range. In Chapter 4 we discuss efficiency measurements made with a sample HEG grating.

[1]This derivation is for so-called scalar diffraction theory. A complete vector treatment of Maxwell's equations gives slightly different results at some energies (see Section 5.3).

[2]There are actually five dips corresponding to the five gold M edges, but MV and MIV are indistinguishable in the figure.

[3]In practice, only one of the first grating diffraction orders must be measured since they are identical throughout the HETGS energy range. At energies significantly below this range, any tilt of the grating causes the grating to act like a waveguide (Ceglio, 1989) with the result of a higher intensity in one of the first grating diffraction orders.

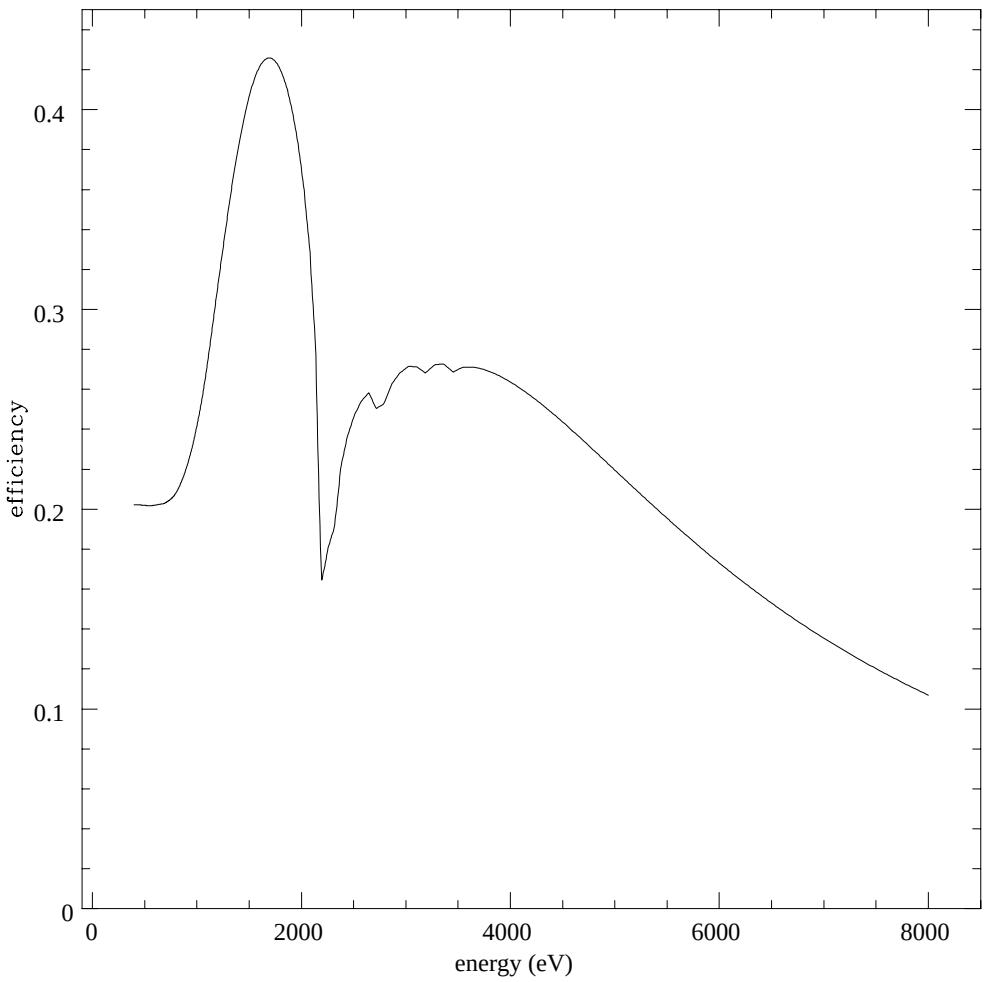

Figure 2-3: Example of gold transmission grating efficiency over entire HETGS energy range, calculated using XRAY. Period of grating is 2000 Å, bar height is 4000 Å, and grating bar thickness is 1000 Å.

Chapter 3

Measurements of Resolving Power at the Daresbury Laboratory Synchrotron Radiation Source

The Daresbury Laboratory Synchrotron Radiation Source uses a linear accelerator for electron acceleration up to 12 MeV. A booster then accelerates the electrons to 600 MeV before they are injected into the storage ring where they reach a maximum energy of about 2 GeV. The synchrotron ring has 11 beam lines with radiation energy ranges spanning from the infra-red to x-ray.

3.1 Goal of Tests

The instrument specification on the resolving power of the HETGS is that it should peak at $(E/\Delta E)\sim 1000$. Consequently, it is important to minimize all of the components that contribute to ΔE, a principal one of which for peak instrumental resolution is the period variation (Canizares *et al.*, 1992).

Measurements of the period variations of HETGS transmission gratings are made at MIT by illuminating $\sim$1 mm^2 patches of grating facets with a laser while monitoring the angle of the diffracted beam. This method has the drawback that it does not measure the real parameter of interest— period variations for transmitted x-ray. An

attempt to measure this parameter was made by Abdali *et al.*, 1993, using a triple axis x-ray diffractometer at the Danish Space Research Institute in June of 1993, but due to the lack of beam intensity at the higher grating diffraction orders and the large rocking curve width of one of the crystals used in the diffractometer, only an upper limit on the period variation of test grating HX101 ($\Delta p/p <$ 4.0E-4) could be made. Using UV laser reflection at the MIT testing facility at the Center for Space Research, $\Delta p/p$ for this same grating was measured as 1.18E-4 rms (Dewey, 1993), (Abdali *et al.*, 1993).

To overcome the intensity problem in higher grating diffraction orders, crystals from the Danish Space Research Institute's crystal diffractometer were used at the Daresbury Laboratory Synchrotron Radiation Source. The goal of this experiment was to measure the $\Delta p/p$ of HX101 for x-ray transmission.

3.2 Test Procedure

The period variation measurement experiment was performed on beam line 8.4, during the period of November 27–30, 1993. Our research crew consisted of personnel from the Danish Space Research Institute, the Space Research Institute at the Russian Academy of Sciences, the Smithsonian Astrophysical Observatory, and MIT's Center for Space Research. The experimental set-up is shown below in Figure 3-1.

White beam— with a height of ~1 mm and a width of ~7 mm— from the synchrotron was incident on a double, silicon (111) crystal monochromator. The monochromator was calibrated by placing various types of filters in the diffracted beam and locating the absorption edges as the parallel crystals were rotated. After the calibration, we rotated the monochromator to a beam incidence angle of 13.564 degrees, which corresponds to an energy of 8.442 $\pm$ 0.005 keV.

The diffracted beam from the double crystal monochromator passed through an ionization chamber that was used to monitor variations in the beam intensity. The beam was then incident on a second monochromator consisting of a silicon (444) crystal, which we tuned to the Bragg angle. The beam diffracted by the second

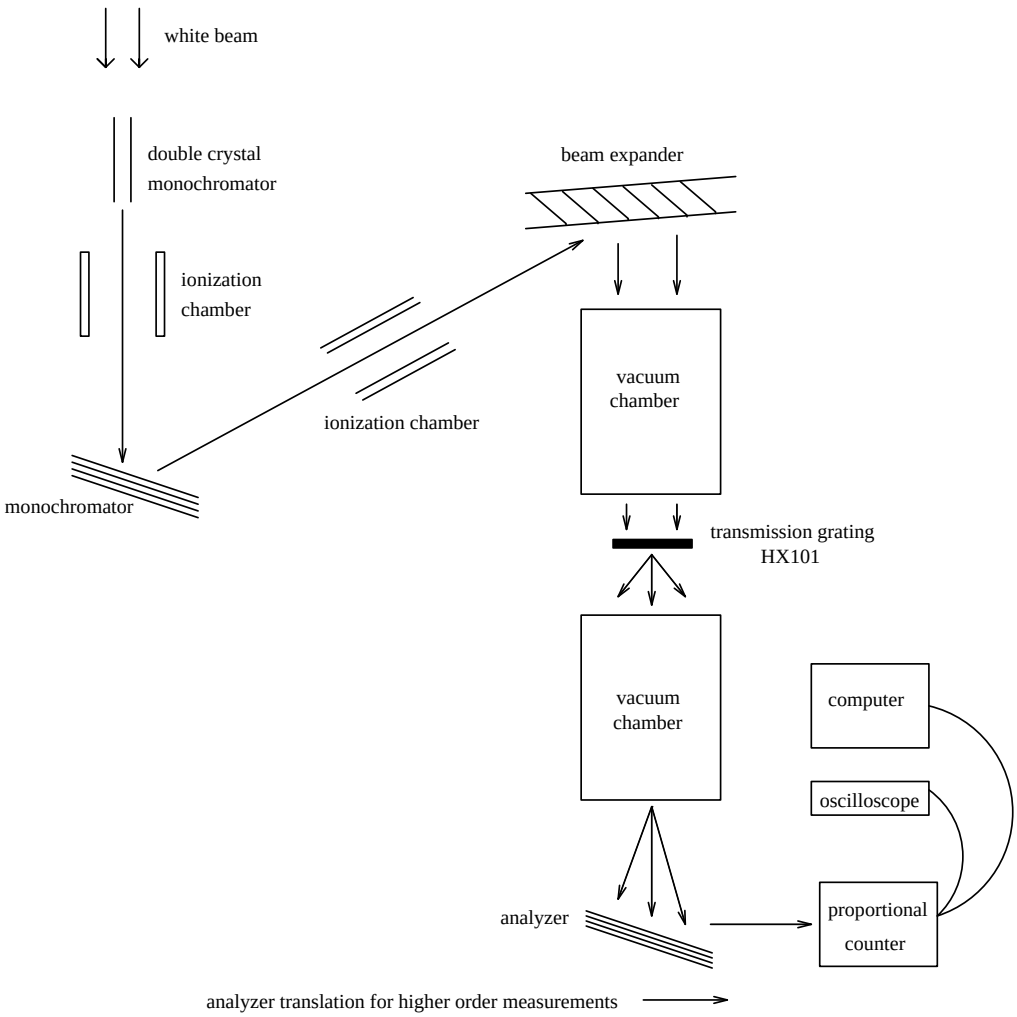

Figure 3-1: Schematic of test set-up at the Synchrotron Radiation Source.

Table 3.1: HX101 parameters as measured at MIT (Dewey, 1993)(Abdali *et al.*, 1993).

period	2001 ± 10 Å
gap width	760 ± 25 Å
bar height	3750 ± 200 Å
$\Delta p/p$ (rms)	1.18E-4

monochromator passed through another ionization chamber. This chamber was used for re-alignment of the second monochromator because small vibrations in the x-ray hutch were sufficient to move the crystal such that the Bragg condition was no longer satisfied.

After traversing the second ionization chamber, the beam was incident on a silicon (444) beam expander crystal. This crystal was asymmetrically-cut with an angle of 57 degrees between the Bragg diffraction planes and the crystal surface. At 8.442 keV, the Bragg angle for the beam expander was 69.44 degrees, which corresponds to a grazing incidence of 12.44 degrees. The beam expansion factor, $\frac{1}{tan(12.44)}$, was ∼4.5 at this angle.

The expanded beam passed through a vacuum chamber (enclosed with thin plastic entrance and exit windows) that reduced beam absorption in the air and the beam was then incident on transmission grating HX101. Nominal grating parameters for HX101 as measured at MIT (Dewey, 1993) (Abdali *et al.*, 1993) are listed above in Table 3.1. The diffracted beam passed through a second vacuum chamber and was incident on a final asymmetrically-cut silicon (444) analyzer crystal. We used this crystal to study the individual orders of the grating diffraction pattern by rocking through the Bragg angle for each order. The beam diffracted by the analyzer crystal was detected by a gas proportional counter.

In order to align the grating such that it was normal to the incident beam, we performed a test in which the grating was tilted ±20 degrees about its initial tilt (which we estimated to be less than a degree from normal to the beam) while the grating's first order intensity was monitored. Because of the ∼3:1 aspect ratio of the

grating bars of HX101, the first order intensity is expected to fall off rapidly until reaching zero when the tilt is equal to $tan^{-1}(p/h)$, where p is the grating period and h is the grating bar height. We estimated the tilt angle corresponding to the peak first order intensity and rotated the grating to this angle (which was later determined to be a tilt of $\sim$0.35 degrees from normal) for all subsequent tests. Normal beam incidence was important for maximizing the higher grating diffraction order efficiencies and the 0.35 degree departure from normal incidence is small enough to make an insignificant difference in the higher grating diffraction order efficiencies.

The analysis technique follows the discussion of Section 2.2. Basically, we attempt to compute $\Delta p/p$ according to equation 2.5 (slightly modified to include the effects of the analyzer crystal, $\Delta\theta_c$):

$$\frac{\Delta p}{p} = \frac{1}{tan\theta_m}\sqrt{(\Delta\theta_m)^2 - (\Delta\theta_c)^2 - (\Delta\theta_m^\lambda)^2} \tag{3.1}$$

where θ_m is the dispersion angle of the m^{th} order ($m\lambda = psin\theta$), $\Delta\theta_m$ is the observed width of the narrow feature (FWHM), and $\Delta\theta_c$ and $\Delta\theta_m^\lambda$ are the contributions to this width due to the analyzer crystal and the wavelength spread, respectively.

The λ component of $\Delta\theta$ was measured by replacing the beam expander by a symmetric crystal in an anti-parallel, dispersive arrangement with respect to the monochromator crystal (Christensen *et al.*, 1993). A rocking curve of this symmetric crystal was conducted and the measured width of the rocking curve was related to the wavelength spread using Bragg's Law. The experimental value obtained for $\Delta\lambda/\lambda$ was 5.9($\pm$0.6)E-5 (Christensen, 1994, private communication).

We measured the crystal component of $\Delta\theta$ by rocking the analyzer crystal through the zeroth grating diffraction order and also through the direct beam (where the grating was removed from the set-up). For the zeroth order measurement, the period component of $\Delta\theta$ vanishes because θ_0 is 0 degrees (equation 2.3). Of course, for the direct beam measurement this contribution is also zero because of the absence of the grating. For both the zeroth order and direct beam measurements, $\Delta\lambda/\lambda$ is negligible compared to the observed widths. Therefore, the widths of the zeroth order as well as the direct beam are measurements of $\Delta\theta_c$.

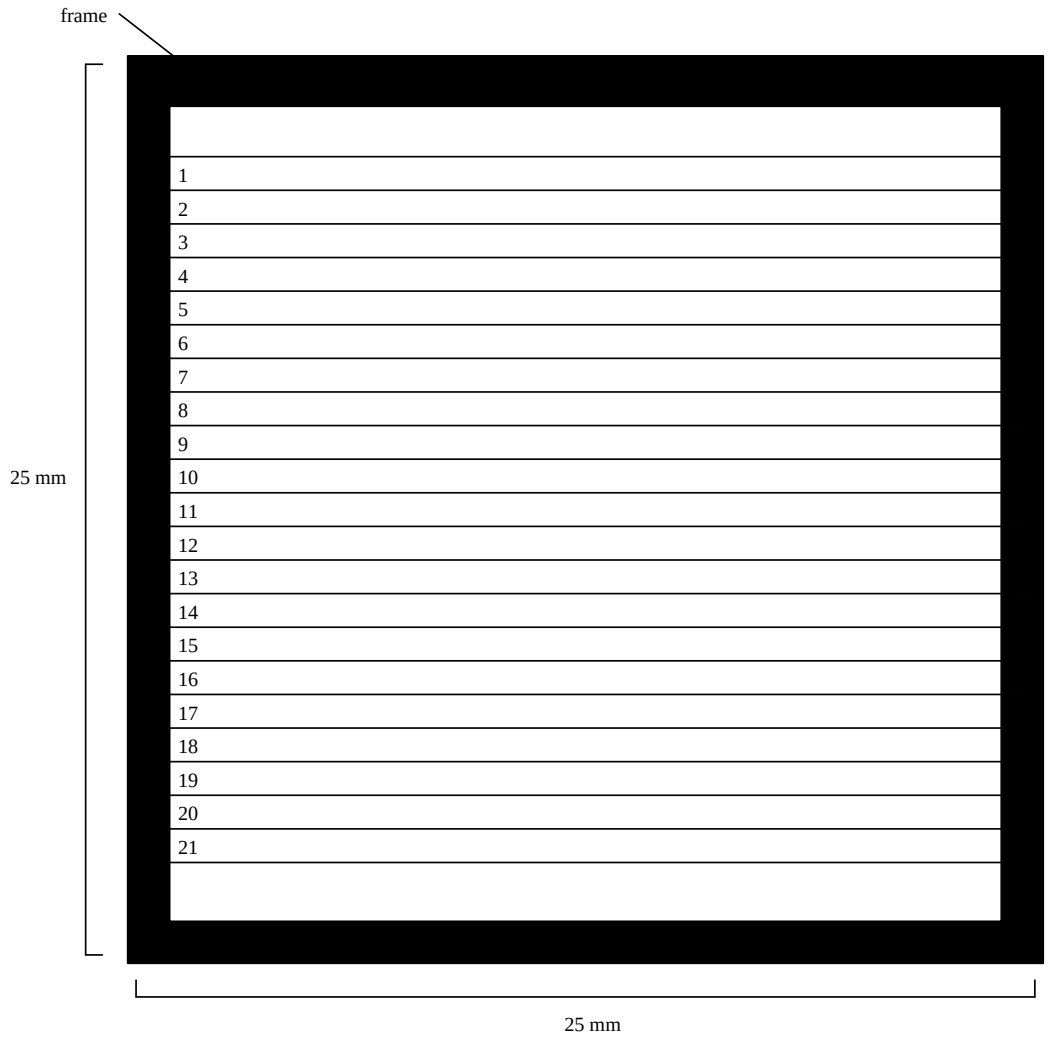

Figure 3-2: HX101 illuminated strips for the twelfth grating diffraction order measurements.

We measured the width of the diffraction order in the twelfth grating diffraction order by rocking the analyzer crystal over the twelfth order peak at 21 different grating positions— as shown above in Figure 3-2. Because the incident beam was expanded nearly five-fold, each test exposed a 1 mm high strip across the entire grating. To ensure that the same part of the analyzer crystal was being used for the zeroth order measurement and all of the twelfth order measurements, the crystal was translated as shown in the bottom of Figure 3-1. This compensation should have eliminated the effects of any analyzer crystal non-uniformities.

3.3 Summary of Data

A plot of a rocking curve through the zeroth order and one of the twelfth order grating positions (histogram with error bars) along with Gaussian fits (solid lines) are shown in Figure 3-3 and 3-4, respectively. Figure 3-3 corresponds to the rocking curve of the zeroth order upon illumination of strip #10, which is shown in Figure 3-2. Each data point involved a ~2 second collection period. Figure 3-4 corresponds to the rocking curve of the twelfth order upon illumination of strip #6. Each data point involved a ~20 second collection period. The abscissa of the two figures is in motor steps where one motor step corresponds to a 0.05 arcsec rotation. The error bars shown in the figures are the square roots of the number of counts.

Gaussian fits with a constant background were made to the data. The full width at half maximum (FWHM) for a direct beam, two zeroth grating diffraction orders, and the twelfth grating diffraction order at different grating heights are shown below in Table 3.2. Also listed are the integration times for each analyzer crystal position. Note that these times are slightly variable as the time of collection was normalized with respect to the beam intensity.

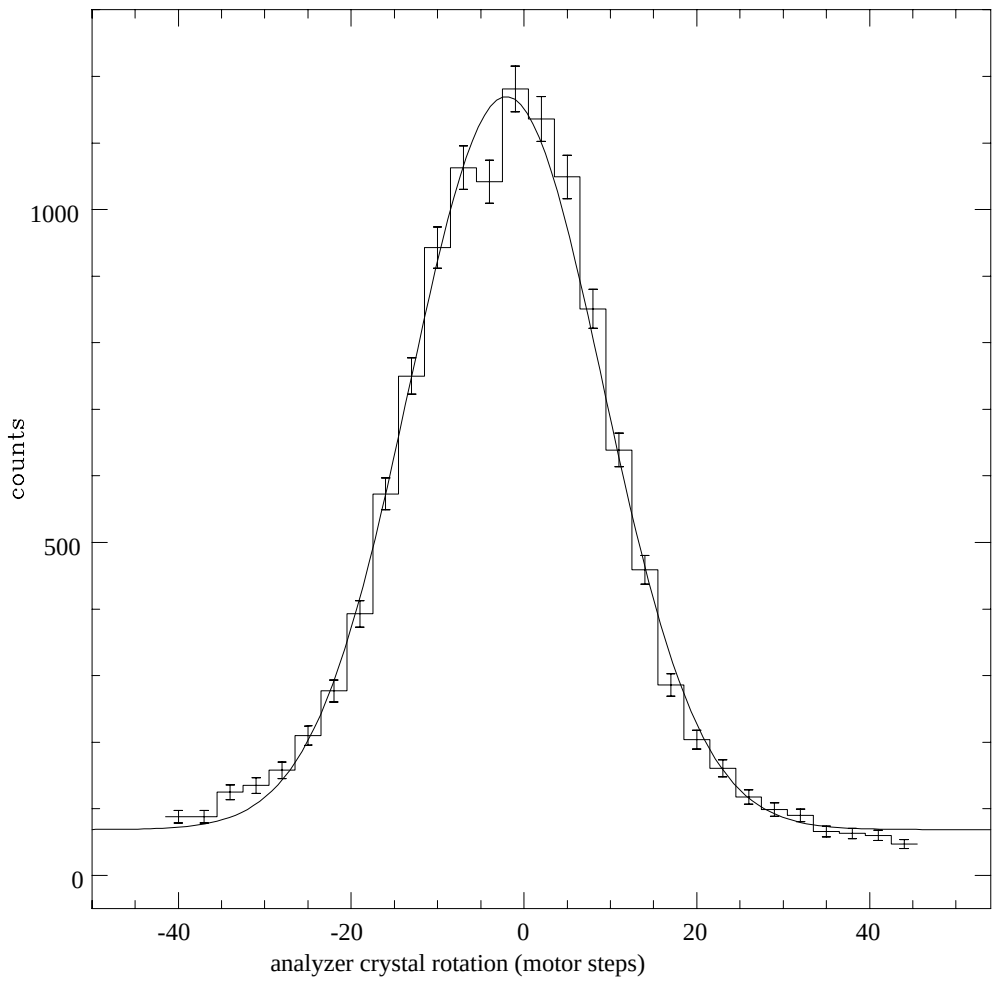

Figure 3-3: Rocking curve of zeroth grating diffraction order. Each data point is for a $\sim$2 second collection at each analyzer crystal position. The solid line is the best Gaussian fit to the data. One motor step is equal to 0.05 arcsec.

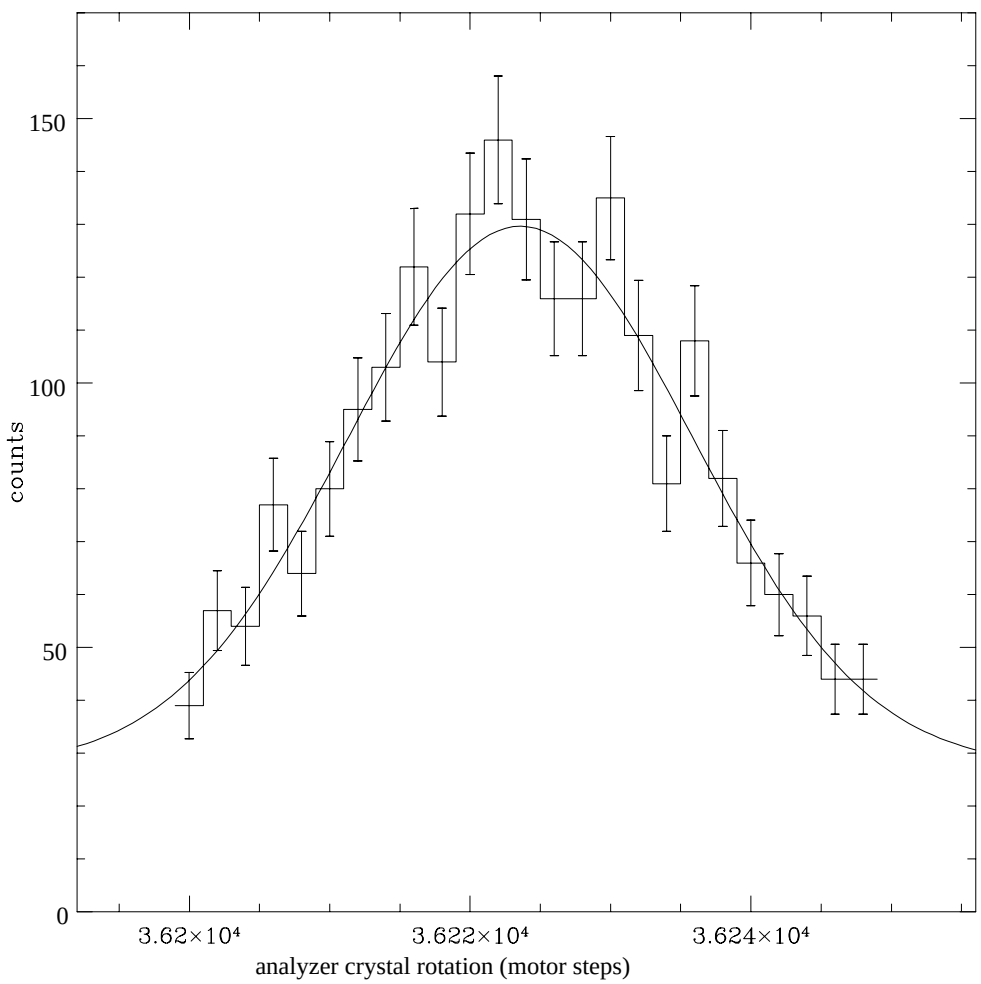

Figure 3-4: Rocking curve of twelfth grating diffraction order at the #6 grating position (see Figure 3-2). Each data point is for a ∼20 second collection at each analyzer crystal position. The solid line is the best Gaussian fit to the data. One motor step is equal to 0.05 arcsec.

Table 3.2: FWHM data of direct beam and zeroth and twelfth grating diffraction orders. The illuminated part of grating is taken from Figure 3-2.

diffraction order	illuminated part of grating	integration time (s)	FWHM (arcsec)
direct beam	NA	5	1.3696 ± 0.0093
0	10	5	1.338 ± 0.017
0	10	2	1.317 ± 0.023
12	1	20	1.40 ± 0.18
12	2	20	1.42 ± 0.17
12	3	20	1.42 ± 0.18
12	4	20	1.43 ± 0.20
12	5	20	1.56 ± 0.27
12	6	20	1.45 ± 0.32
12	7	20	1.51 ± 0.36
12	8	20	1.27 ± 0.18
12	9	20	1.48 ± 0.26
12	10	20	1.26 ± 0.20
12	10	30	1.111 ± 0.065
12	10	20	1.203 ± 0.075
12	11	20	1.30 ± 0.16
12	12	20	1.48 ± 0.20
12	13	20	1.48 ± 0.28
12	14	20	1.64 ± 0.31
12	15	20	1.38 ± 0.28
12	16	20	1.44 ± 0.24
12	17	20	1.59 ± 0.38
12	18	20	1.54 ± 0.35
12	19	20	1.19 ± 0.17
12	20	20	1.53 ± 0.32
12	21	20	1.58 ± 0.46

Table 3.3: $\Delta p/p$ components.

$\Delta p/p$ component	value
θ_{12}	0.50446 degrees
$\Delta\theta_{12}$	1.272 $\pm$ 0.035 arcsec
$\Delta\theta_c$	1.3573 $\pm$ 0.0077 arcsec
$\Delta\theta_{12}^{\lambda}$	0.107 $\pm$ 0.011 arcsec

The $\Delta\theta_c$ component of equation 3.1 was calculated by taking a weighted average (Bevington, 1969) of the direct beam measurement and the two zeroth order measurements. I find the average FWHM of these three measurements to be 1.3573 $\pm$ 0.0077 arcsec. The $\Delta\theta_{12}$ component of equation 3.1 was calculated by taking a weighted average (Bevington, 1969) of the twelfth order measurements. I find the average FWHM of these 23 measurements to be 1.272 $\pm$ 0.035 arcsec.

The twelfth order average is significantly less ($\sim 2.5\sigma$) than the direct beam/zeroth order measurement. If the twelfth order data ($\Delta\theta_{12}$) is given by equation 2.4, it is impossible (mathematically) for $\Delta\theta_{12}$ to be less than $\Delta\theta_c$. We have been unable to account for this discrepancy although it is possible that the direct beam/zeroth order measurements include contaminant photons in energies other than those measured at twelfth order. Since the twelfth order FWHM average is un-physical, only an upper limit on the period variation can be determined. The components necessary for calculating that upper limit on $\Delta p/p$ are shown above in Table 3.3.

To obtain a 3σ upper limit, the conservative approach is to subtract 3σ from the $\Delta\theta_c$ measurement and add 3σ to the $\Delta\theta_{12}$ measurement. This results in a $\Delta\theta_c$ equal to 1.3342 arcsec and $\Delta\theta_{12}$ equal to 1.377 arcsec. Using equation 3.1 with $m = 12$, this corresponds to a 3σ upper limit on $\Delta p/p$ of 1.8E-4.

3.4 Conclusions

Our investigation of transmission grating HX101's resolution was limited by the fact that the crystal's resolution and the grating's efficiency were optimized at different energies. That is, in order to get a reasonable intensity in the higher grating diffraction orders, the incident wavelength had to be increased and this caused an increase in the crystal component of $\Delta\theta$.[1] The end result was that the crystal component dominated the FWHM of the twelfth grating diffraction order so that only an upper limit on $\Delta p/p$ could be determined. This upper limit is lower than the Abdali *et al.* measurement made in June 1993 and is consistent with the specification for $\Delta p/p$ required for the HETG (Markert, 1994, private communication).

Another result that can be obtained from this round of tests has to do with period variation uniformity. Figure 3-5 below shows the FHWM's of the twelfth orders for each of the 21 grating positions (as defined by Figure 3-2). As can be seen in the figure, most of the scans tend to have larger FWHM's than the computed average. This is due to the domination of the average by the two central (strip #10) scans. One of these central scans had a longer integration period and both had more measurements of the background, so better fits to the data were made. To remove the domination of the strip #10 scans, an additional average in which just the short scans at the 21 positions are used should be made. Taking this average, we obtain $\Delta\theta_m$ = 1.397 $\pm$ 0.050 arcsec and a $\Delta p/p$ of 1.7 ($\pm$1.2) E-4, where the uncertainty was calculated using the following formula (Bevington, 1969):

$$(\sigma_{\Delta p/p})^2 = \frac{(\sigma_{\Delta\theta_{12}})^2(\Delta\theta_{12})^2 + (\sigma_{\Delta\theta_c})^2(\Delta\theta_c)^2 + (\sigma_{\Delta\theta_{12}^{\lambda}})^2(\Delta\theta_{12}^{\lambda})^2}{tan^2(\theta_{12})[(\Delta\theta_{12})^2 - (\Delta\theta_c)^2 - (\Delta\theta_{12}^{\lambda})^2]}. \qquad (3.2)$$

This $\Delta p/p$ value is in agreement with the UV laser measurement performed at MIT.

The trends of the measured FWHM's shown in Figure 3-5 can also be compared to the period variation as measured at MIT using the UV laser reflection facility. A contour plot of the period variation of HX101— as measured by Dan Dewey— is

[1] Longer wavelengths also meant an increase in x-ray absorption in the air, which caused a reduction in beam intensity.

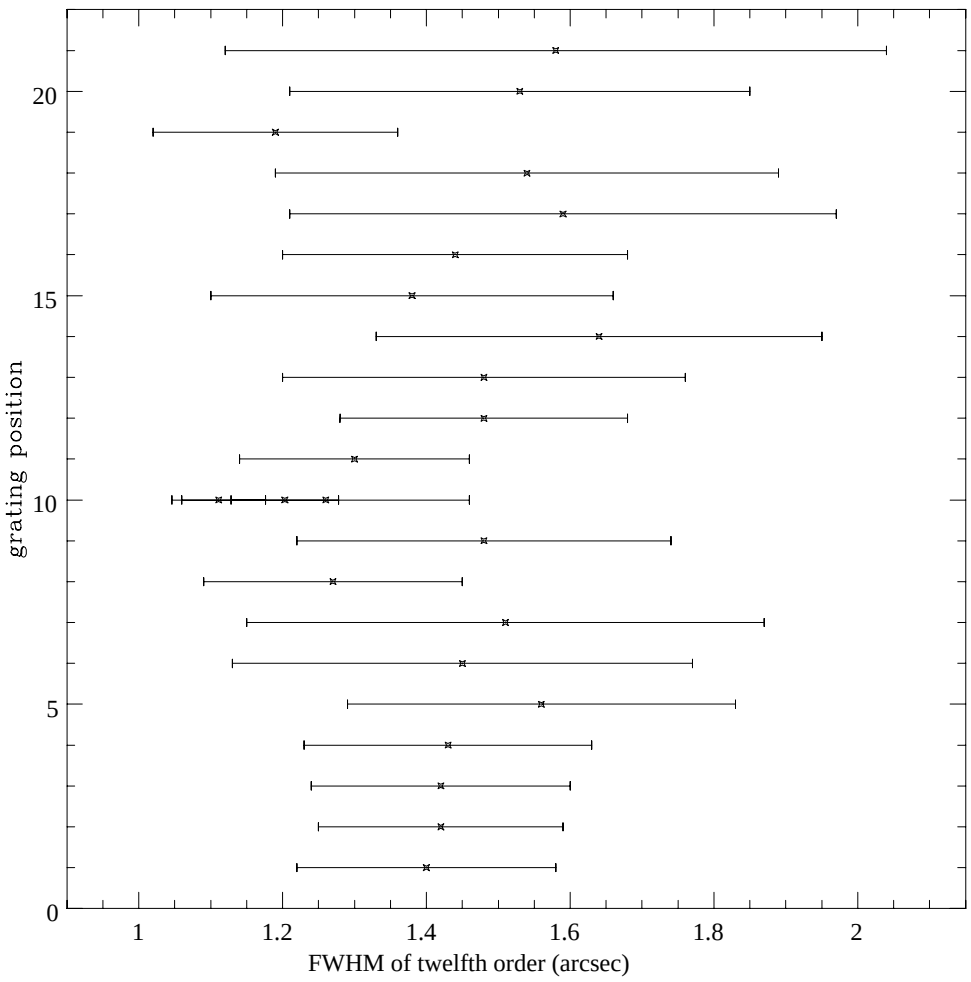

Figure 3-5: FWHM's of twelfth grating diffraction orders for the 21 grating strips as defined by Figure 3-2.

shown below in Figure 3-6. For comparison, the Y-grating position of about 12–13 mm corresponds to strip #10 in Figure 3-5. (A complicating factor is that we do not know if higher Y-grating position corresponds to higher strip # as the orientation of the grating for the tests was not recorded. However, 12–13 mm is the center of the grating and this strip is therefore independent of the grating's orientation.)

It is difficult to make a prediction about the expected FWHM's of horizontal 1 mm high strips based on Figure 3-6. Although the contour lines are closer together at higher Y-grating positions, they are also roughly horizontal. This means that the period of a given horizontal strip— though varying widely from the average period of the grating— might have little period variation within the strip itself. It is not possible to overcome this by merely adding up the scans to make a composite scan because there is some slop in the analyzer crystal motor which results in a drift of the actual motor step positions. This suggests that the strip method of testing that was used at the Synchrotron Radiation Source may not be the most effective means of measuring the rms period variation of a grating. Real-time grating motion— so that the entire grating is exposed to the beam during a single scan— would result in a better measurement.

The next step in measuring grating period variation must make use of an analyzing crystal with higher resolution— for example, a channel-cut crystal (as was also proposed by Abdali *et al.*, 1993). In a channel-cut crystal, multiple reflections of an incident beam result in a rocking curve FWHM of a few tenths of arcseconds. Such a width would no longer dominate the $\Delta\theta$ of a grating diffraction order of $m \geq 10$ and an accurate measurement of the period variation of transmitted x-rays could be made.

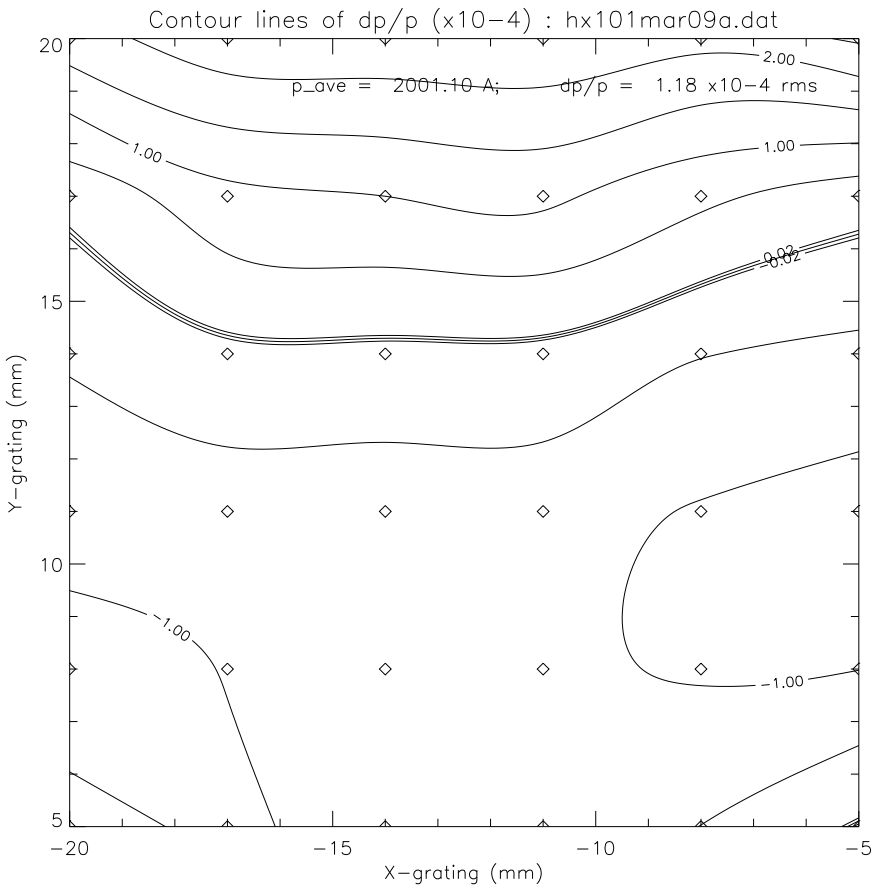

Figure 3-6: Contour plot of the period variation of test grating HX101 as measured by Dan Dewey at the MIT laser reflection facility.

Chapter 4

Measurements of Efficiency at the National Synchrotron Light Source

The National Synchrotron Light Source (NSLS) is located at Brookhaven National Laboratory in Upton, New York. It includes both a vacuum ultraviolet (VUV) ring with 17 beam ports and an x-ray ring with 30 beam ports. The VUV ring operates at an electron energy optimized for radiation in the energy range of 1 eV to 1 keV. The x-ray ring operates at an electron energy optimized for radiation in the 1–20 keV energy range. A floor plan of the synchrotron is shown below in Figure 4-1 (NSLS Experimenter's Handbook, 1992).

4.1 Goal of Tests

One of the instrument specifications of the HETGS is to know the diffraction efficiency of the array of grating facets to 3%[1]. As one step in the pursuit of this ultimate instrumental goal, the goal for the NSLS tests was to measure the efficiency of an individual HETGS facet to 1%. With this accomplished, a related second objective would be to use the measured diffraction efficiencies to obtain a better theoretical

[1]As mentioned in Section 1.3, the 3% value is preliminary.

Figure 4-1: Floor plan of the National Synchrotron Light Source.

model by varying model parameters until good agreement with the data is achieved. This improved theoretical model could include changes in the grating parameters, gold optical constants, or shape of the grating bars.

An additional goal of the NSLS tests is to measure the diffraction efficiencies of several flight quality gratings in detail. These "well-known" gratings can then be used as calibration transfer standards for x-ray tests (as explained in Chapter 1.2), which will be performed at MIT. Although this goal cannot be accomplished at this time since no flight quality gratings have been fabricated, synchrotron tests of existing gratings could give an indication of the feasability of accomplishing this goal in future tests.

4.2 Test History

During the period of July 23–29, 1993, tests on grating facet HX101 were conducted at the NSLS. Beamline X8A, which has an energy range of 0.26–7 keV, was used for these tests[2]. Grating data were collected at 122 different energies in the energy range of 0.8–7 keV. Due to problems with the normalization of the data, efficiencies could only be calculated in the energy range of 2.03–4 keV. These efficiencies are shown below in Figure 4-2. Note that both first orders are included in the efficiency values.

One of the major problems with the July tests was the crudeness of the slit that was used on the detector. This slit consisted of two, 62 mil (0.062 inches) thick, machined-edged steel plates set at a spacing of 1.5 mils with a feeler gauge and glued onto the face of the detector. The slit was later found— with the use of a microscope— to have a variable width and a difference in height of the slit sides.

Another related problem with the July tests was a lack of normalization data (i.e., the slitted detector and the monitor detector were not fully cross-calibrated). Since constant detector slit size and detector efficiencies were assumed, only three

[2] A schematic of the test set-up is shown in Figure 4-3, with one modification— the detector block in Figure 4-3 was equipped with a 1.5 mil (0.0015 inches) slitted detector and an un-slitted detector for the July 1993 tests.

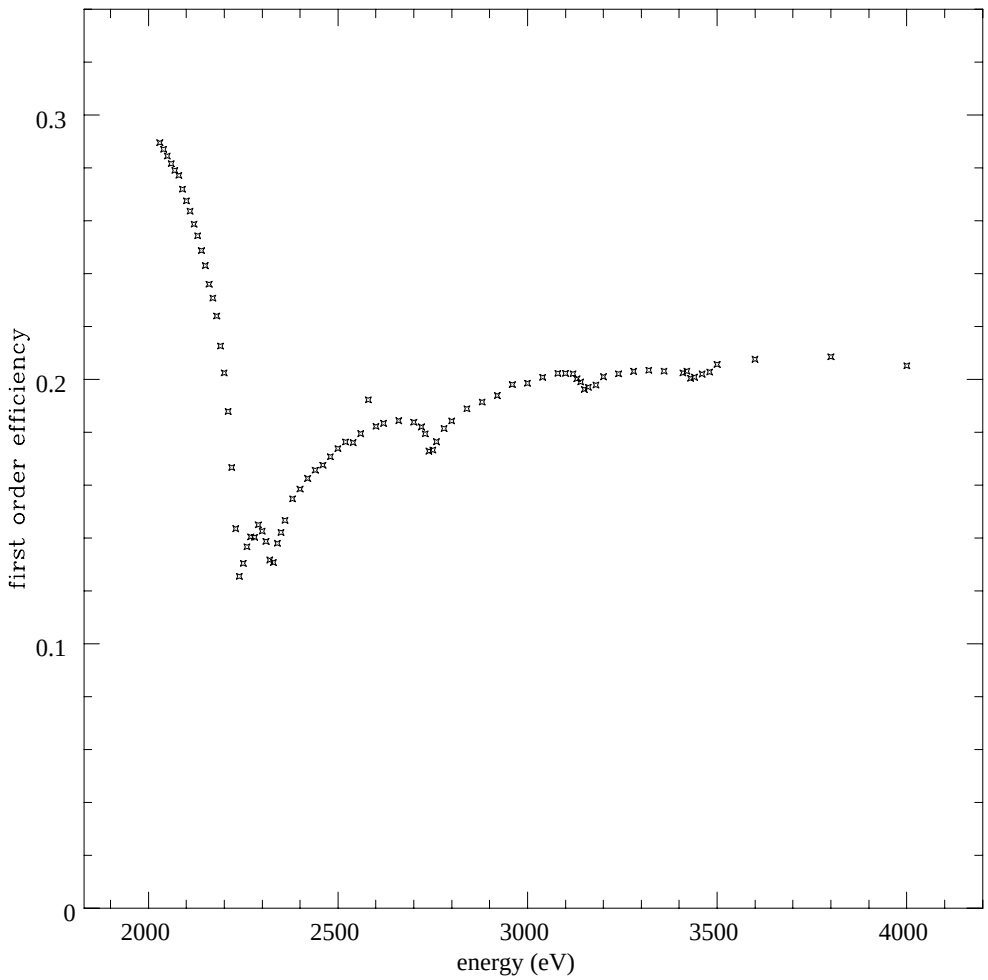

Figure 4-2: July 1993, first order efficiency measurements.

normalization scans for 84 grating efficiency scans in the 2.03–4 keV energy range were conducted. In fact, as we discovered in subsequent tests, the extrapolation to the other energies that was necessary was highly uncertain because it was not based on much data (see Section 4.4.2 for a discussion of the detector normalization technique).

To overcome the normalization problems encountered in the July 1993 tests, two changes were suggested for future tests— the crude detector slit should be replaced and additional normalization scans should be carried out. These changes were made for a second round of synchrotron tests of HX101, which were conducted on the same beam line during the period of January 17–21, 1994.

4.3 Test Set-up

A schematic diagram of the test set-up at the downstream end of beam line X8A is shown below in Figure 4-3. White beam from the synchrotron was incident on the monochromator, which is upstream from the test chamber and not shown in Figure 4-3. The monochromator crystals that were used for the grating tests were a pair of silicon (111) crystals and a pair of multi-layer crystals. To set the width of the monochromatic x-ray beam, two slits— one upstream (called the AC jaws) and downstream (shown at the far right of Figure 4-3)— were necessary because the beam has been found to have a focused and an unfocused portion. The downstream slits are adequate for setting the width of the unfocused portion of the beam, but the beam has been observed to come to a focus near the position of the downstream slits (Graessle, 1994, private communication). Therefore, the upstream AC jaws are necessary to limit the size of the focused portion of the beam.

The test chamber was mounted on a table equipped with linear motors that moved the table perpendicular to the x-ray beam in order to maximize the x-ray intensity. The grating was held in a fixture that could be rotated about its center in steps of 0.9 arcsec. The detector block also had a rotation (about the center of the grating fixture) resolution of 0.9 arcsec. The two detectors on the detector block were 176.6 $\pm$ 1.0 mm from their axis of rotation.

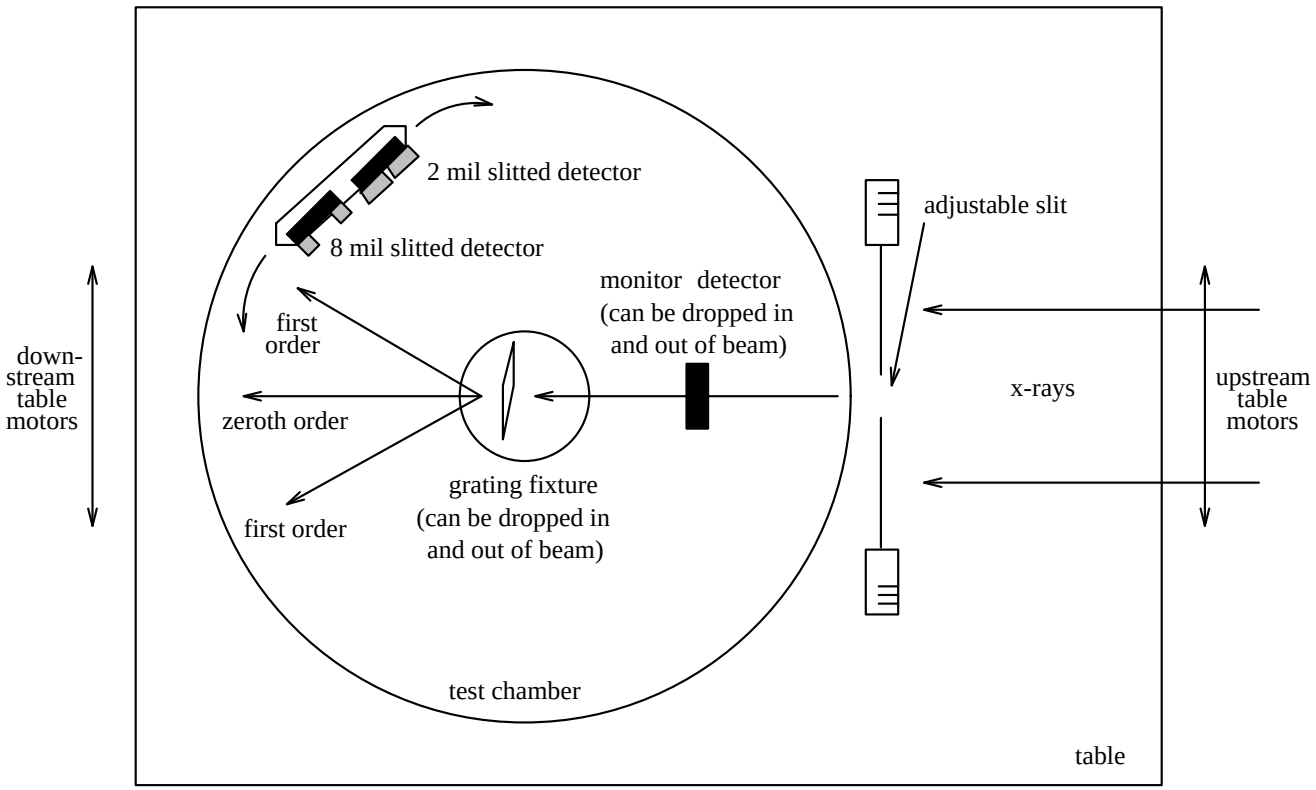

Figure 4-3: Test set-up at downstream section of beam line X8A.

The three detectors in the chamber— the monitor and the two slitted detectors— were AXUV-100 silicon diodes, made by International Radiation Detectors. The detectors all have an active area of $\sim$1 cm^2, but the two detectors on the detector block were covered by slit fixtures. The two sizes of slits used were $\sim$2 mils and $\sim$8 mils. The 2 mil slit was made by cutting into a 15 mil thick, steel sheet with a 2 mil thick, saw blade. The 8 mil slit was made by setting the distance between two steel plates with an 8 mil feeler gauge.

4.4 January 1994 Preliminary Tests

4.4.1 Verifying Test Configuration

The preliminary tests that were conducted included measuring the beam width (with the grating removed) using the 2 mil slitted detector, measuring and minimizing the tilt from normal incidence of the grating, and testing the repeatability of motions of the 2 mil slitted detector. The beam width (which was kept constant for all tests) was measured as $\sim$5 mils at an energy of 2.03 keV. The residual tilt from normal incidence of the grating after adjustments were made was 0.15 ± 0.06 degrees. Repeatability tests of the 2 mil slitted detector motion eliminated any worries that stress on the detector wires would move the diode slightly and thus introduce an error into the computed intensity.

In order to measure the efficiencies, monitor detector readings were required as a measurement of the intensity of the beam incident on the grating. Besides these measurements, two additional pieces of information— the relative efficiencies of the monitor detector and slitted detectors and the precise size of the 2 mil slit— were required to measure absolute efficiencies.

4.4.2 Detector Cross-Calibration

The 8 mil slitted detector was calibrated with respect to the monitor detector at 24 different energies. This was the detector normalization procedure, which we had failed

to do adequately in the July 1993 tests (see Section 4.2). Since the beam was merely ~5 mils wide, the 8 mil, slitted detector was stepped through the beam until the current reading of the detector was maximized (i.e. when the entire beam was within the slit). Then the readings of the monitor detector and the slitted detector could be directly compared. The ratios of the slitted detector readings to the monitor detector readings at the 24 energies are shown below in Figure 4-4, along with a second order polynomial fit to the data. Since the detectors are all essentially identical, it is not surprising that the ratios are nearly unity. However, since we want the calibration to be accurate to better than 1%, it is important to make the relatively small correction.

The 2 mil slitted detector was calibrated with respect to the monitor detector in the two energy ranges for which it would be used for grating tests— $\leq$2 keV and $\geq$4 keV.[3] At distinct energies, the beam was mapped with the 2 mil, slitted detector (while also taking monitor detector readings) by stepping through the beam in steps slightly smaller than the size of the slit. The ratios of the slitted detector to monitor detector readings were then summed up over the mapping. If the slitted detector step size had been the same as the size of the slit and the slitted detector and monitor detector had had identical efficiencies, the ratio sums would have been equal to unity. So the calculated ratio sums contain the information of both the slit size and the deviation between the slitted detector and monitor detector efficiencies. The summed ratios for the low and high energy ranges are shown in Figures 4-5 and 4-6, respectively, along with second order polynomial fits to the data.

The silicon monochromator crystals were used to select energies in the range of 2.03–6.6 keV, with an uncertainty of $\pm$5 eV. In the lower part of this energy range (2.03–4.2 keV), the grating diffraction orders were separated by more than 8 mils. To take advantage of this fact, the 8 mil slitted detector was used to step through the zeroth order and also the first order until the entire order was within the slit. Then, by comparing the slitted detector reading to the monitor detector reading— and using the detector calibration data described above— the absolute zeroth and

[3]One additional calibration scan was also conducted in between these two energy ranges at 2.83 keV. It was used to extrapolate the normalization to the higher energy range.

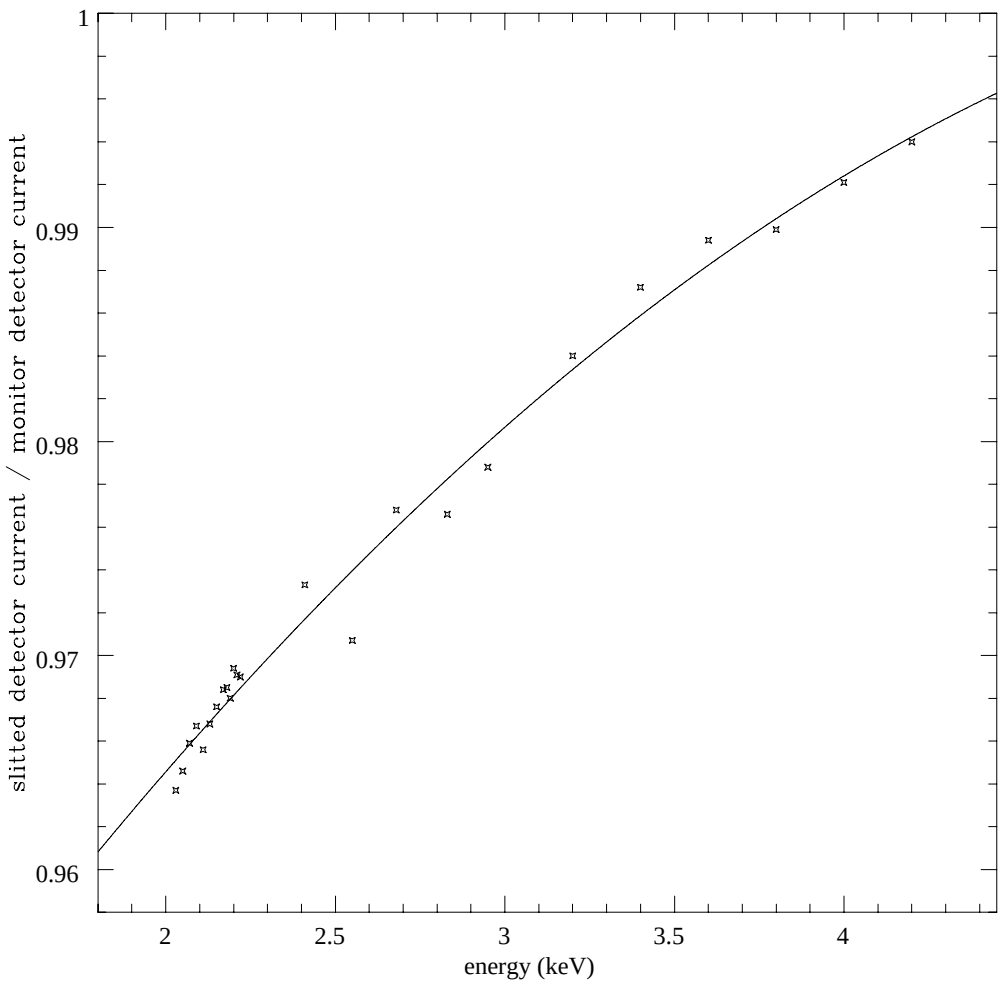

Figure 4-4: 2.03–4.2 keV slitted detector and monitor detector calibration results.

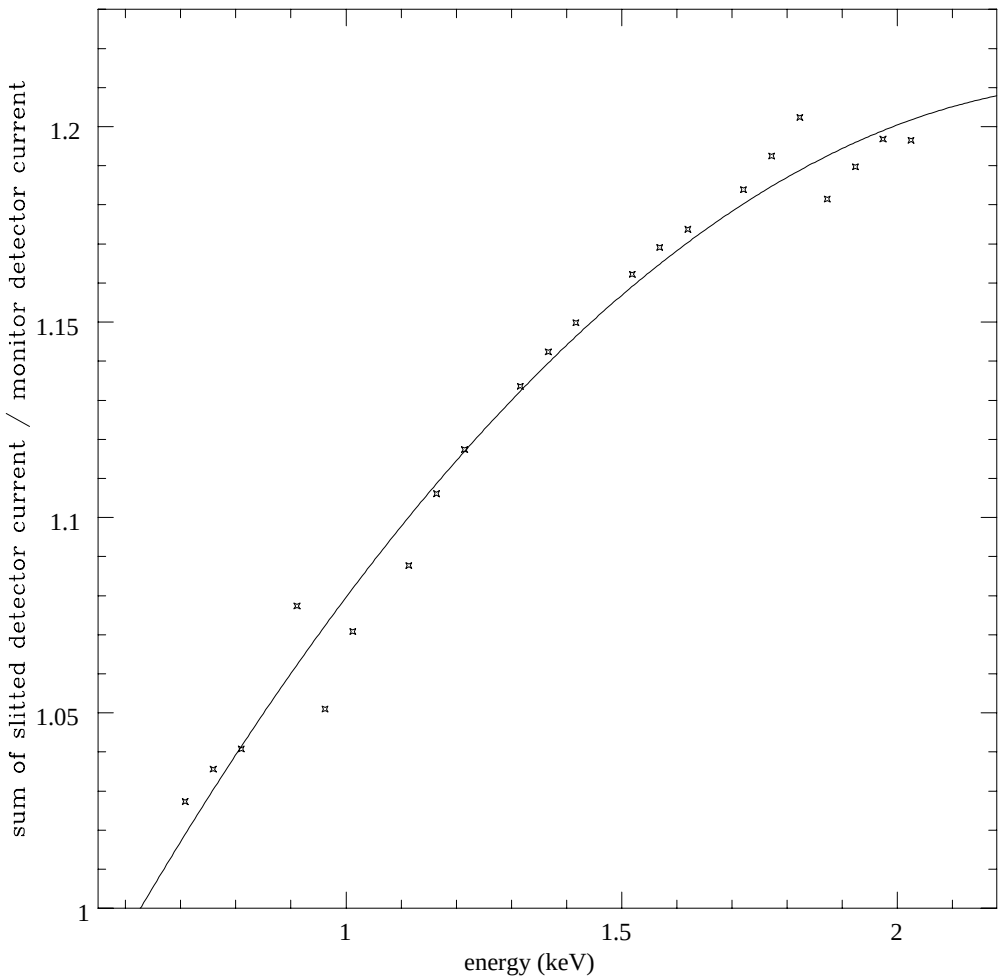

Figure 4-5: 0.708–2.025 keV slitted detector and monitor detector calibration results.

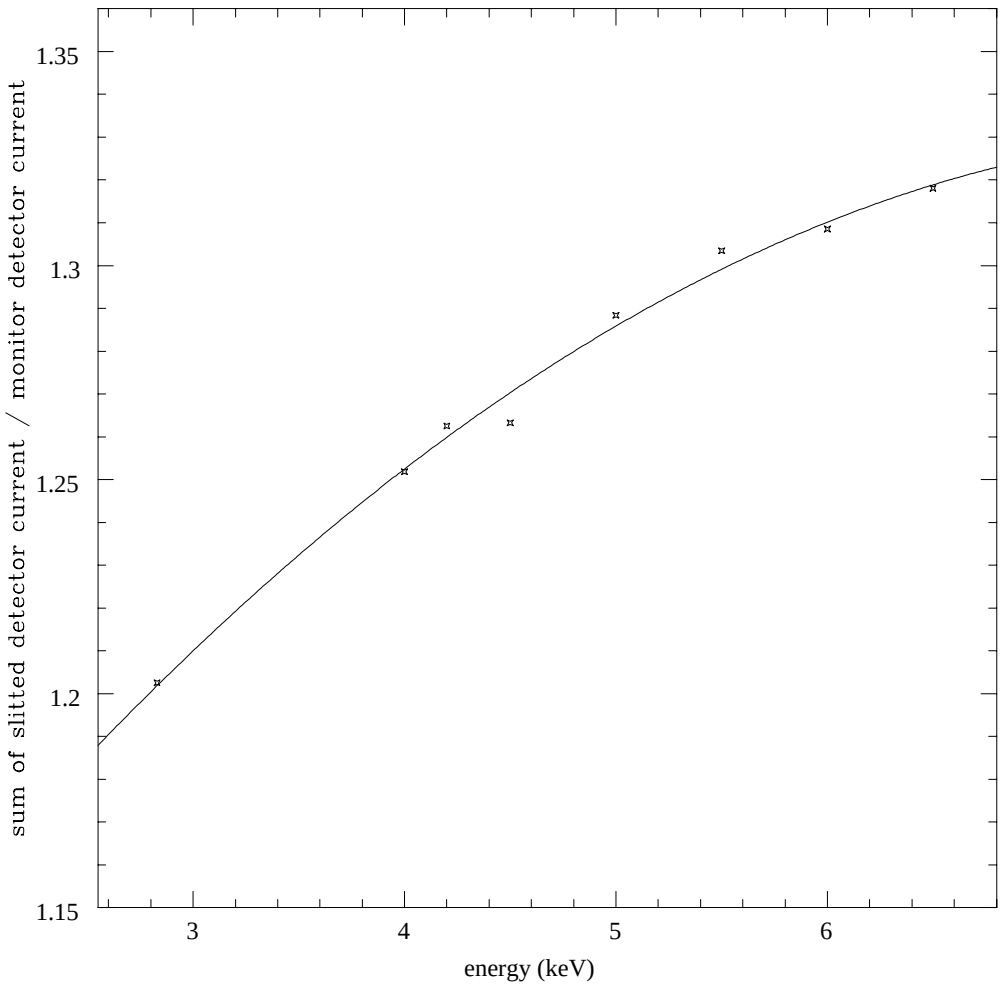

Figure 4-6: 2.83–6.5 keV slitted detector and monitor detector calibration results. The detector cross-calibration scans were actually conducted in 5 and 10 motor step intervals of the slitted detector. Because all efficiency tests were conducted in 40 motor step intervals, the calculated ratios were normalized by dividing by 8 or 4 in order for the ratios to approach unity and also to facilitate easier comparison with Figure 4-4 and 4-5.

first order efficiencies could be immediately calculated.

For energies of 4 keV and higher at which the separation between grating diffraction orders is $\leq$ 8 mils, the 2 mil slitted detector was used to map out the zeroth and first orders. The slitted detector was moved in steps slightly smaller than the size of its slit, and both slitted detector and monitor detector readings were recorded.

The multi-layer monochromator crystals were used to select energies in the range of 0.7–2 keV. These crystals are made of layers of tungsten and silicon, with a 2d spacing of 50 Å. The energy scale of this monochromator was calibrated by Jiahong Zhang in January 1994. She used filters of different materials to find absorption edges as a function of crystal angular position.

Although the separation of grating diffraction orders in the 0.7–2 keV energy range is much greater than 8 mils, the 8 mil slitted detector could not be used to measure the zeroth and first order efficiencies (the technique used in the 2.03–4.2 keV energy range) because of the low spectral resolution of the multi-layer crystals[4]. The larger angular size of the beam from the monochromator crystals resulted in grating diffraction orders with long and often overlapping tails. Individual grating diffraction orders could not be isolated within an 8 mil slit because of the size of the tails. So the method used for measuring the zeroth and first order efficiencies in this energy range was the same as that which was used for energies above 4 keV— that is, the 2 mil slitted detector was used to map out the orders.

Approximately 120 tests of transmission grating efficiency were planned with the bulk number of the tests ($\sim$80) in the 2–3.5 keV energy range. This energy range spans the five gold M edges— where sharp features in the first order efficiency were expected. Around these edges, tests were planned in 10 eV increments.

To summarize the test plan, Table 4.1 below lists the equipment used and number of tests planned in the three energy ranges for which zeroth and first order efficiencies were to be measured.

[4]The multi-layer crystals' resolution is $\sim$50 compared to the silicon crystals' resolution of $\sim$2000 (NSLS User's Manual, 1991).

Table 4.1: Equipment and number of tests planned for efficiency measurements.

energy range (keV)	monochromator	detector type	# of tests planned
0.7–2	multi-layer	2 mil, slitted	~20
2.03–4.2	silicon (111)	8 mil, slitted	~80
4.0–6.6	silicon (111)	2 mil, slitted	~20

4.5 Efficiency Test Results

The actual number of grating efficiency tests conducted in the three energy ranges was 21 in the 0.708–2.025 keV energy range, 82 in the 2.03–4.2 keV energy range, and 14 in the 4.0–6.6 keV energy range. Examples of the raw slitted detector scans in the three energy ranges are shown below in Figures 4-7, 4-8, and 4-9. The energies of the three figures are 1.417 keV, 2.5 keV, and 5.6 keV, respectively. In all three figures, the left peak is the zeroth grating diffraction order and the right peak is the first grating diffraction order.

The first step in the calculation of the zeroth and first order efficiencies was to subtract the slitted detector background from the slitted detector readings. This background was measured at every slitted detector position at the same time as the monitor detector was dropped into the beam (as the monitor detector blocked the beam) and used to measure the intensity of the beam incident on the grating. The next step was to divide the background-subtracted, slitted detector currents by the monitor detector currents. The final step in the calculation of the zeroth and first order efficiencies varied depending upon the type of monochromator and slitted detector used for the measurements.

For the 2.03–4.2 keV energy range, the highest slitted detector current to monitor detector current ratio of both the zeroth and first orders were the preliminary, unnormalized efficiencies. These efficiencies were then normalized by dividing by the second order polynomial (shown earlier in Figure 4-4), which was a fit to the 8 mil slitted detector calibration data.

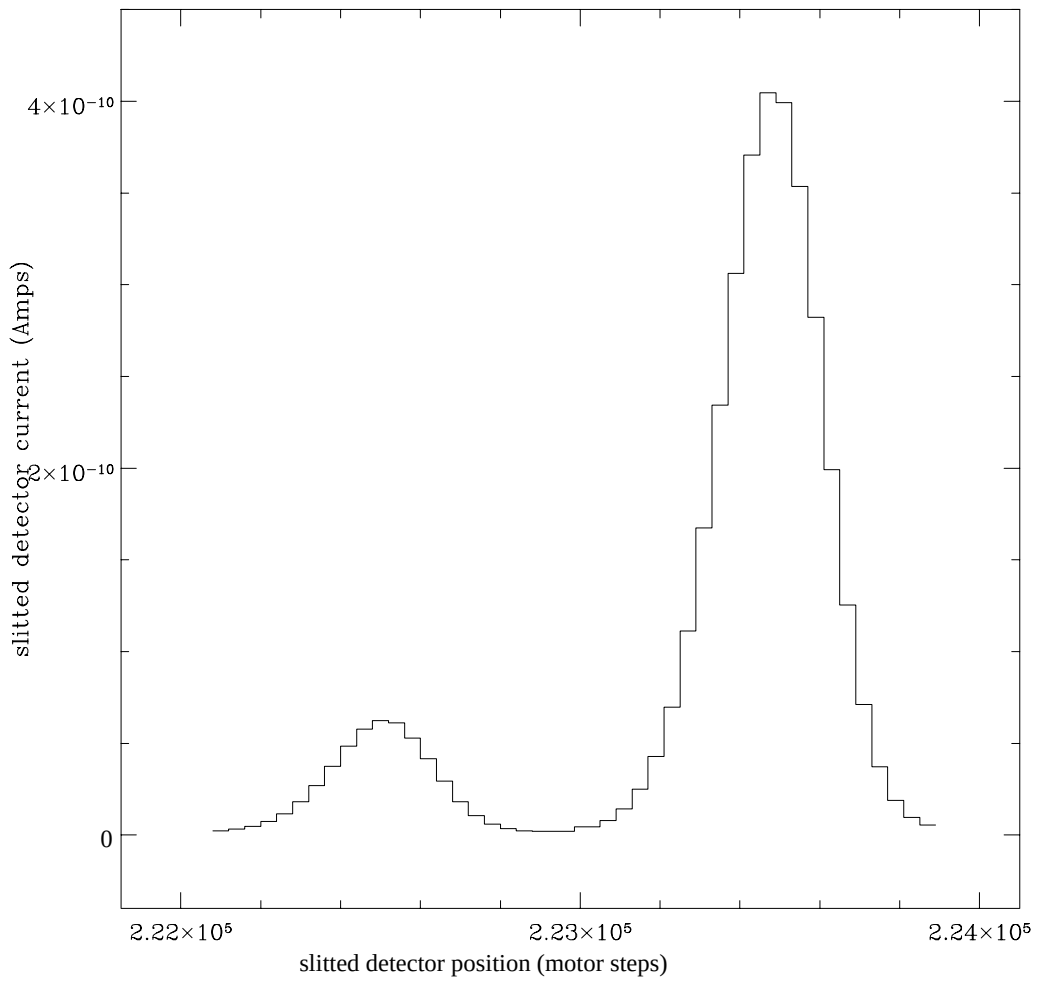

Figure 4-7: 2 mil slitted detector scan at 1.417 keV. Zeroth grating diffraction order on left and first grating diffraction order on right.

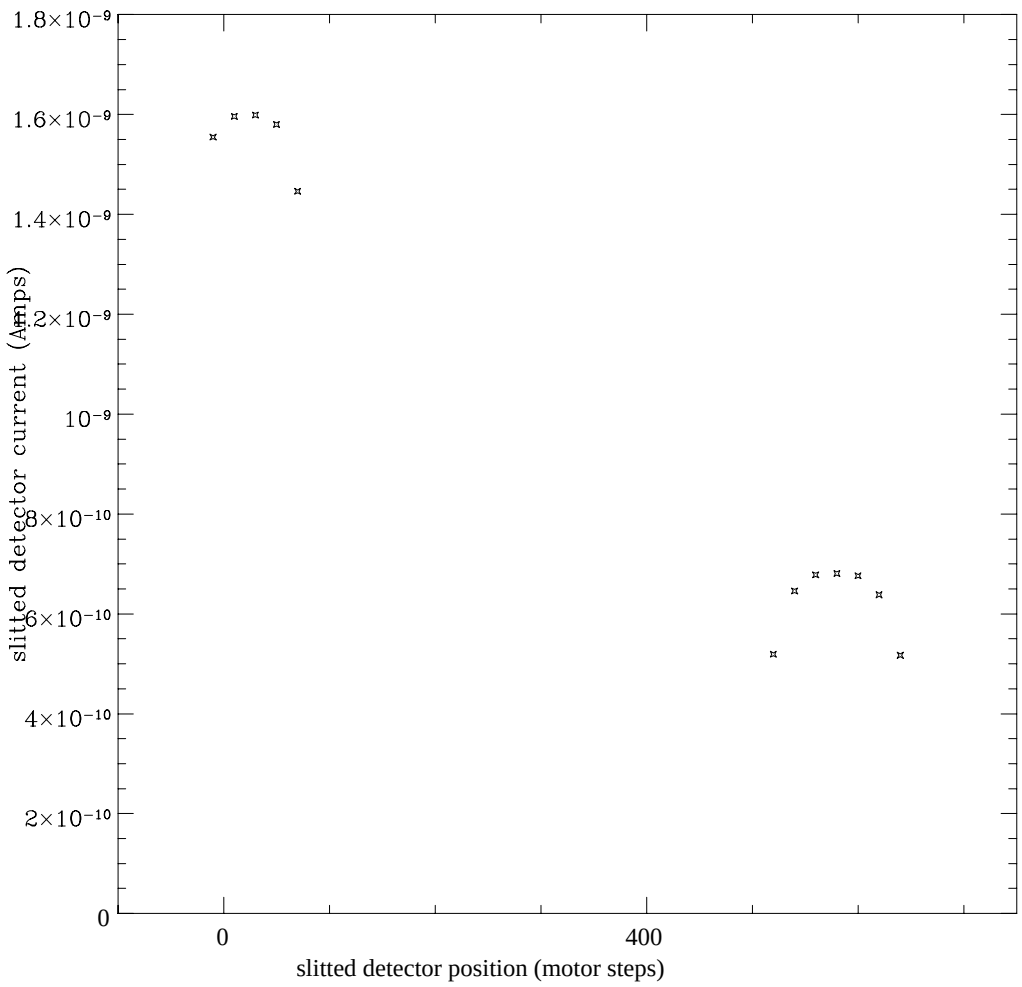

Figure 4-8: 8 mil slitted detector scan at 2.5 keV. Zeroth grating diffraction order on left and first grating diffraction order on right.

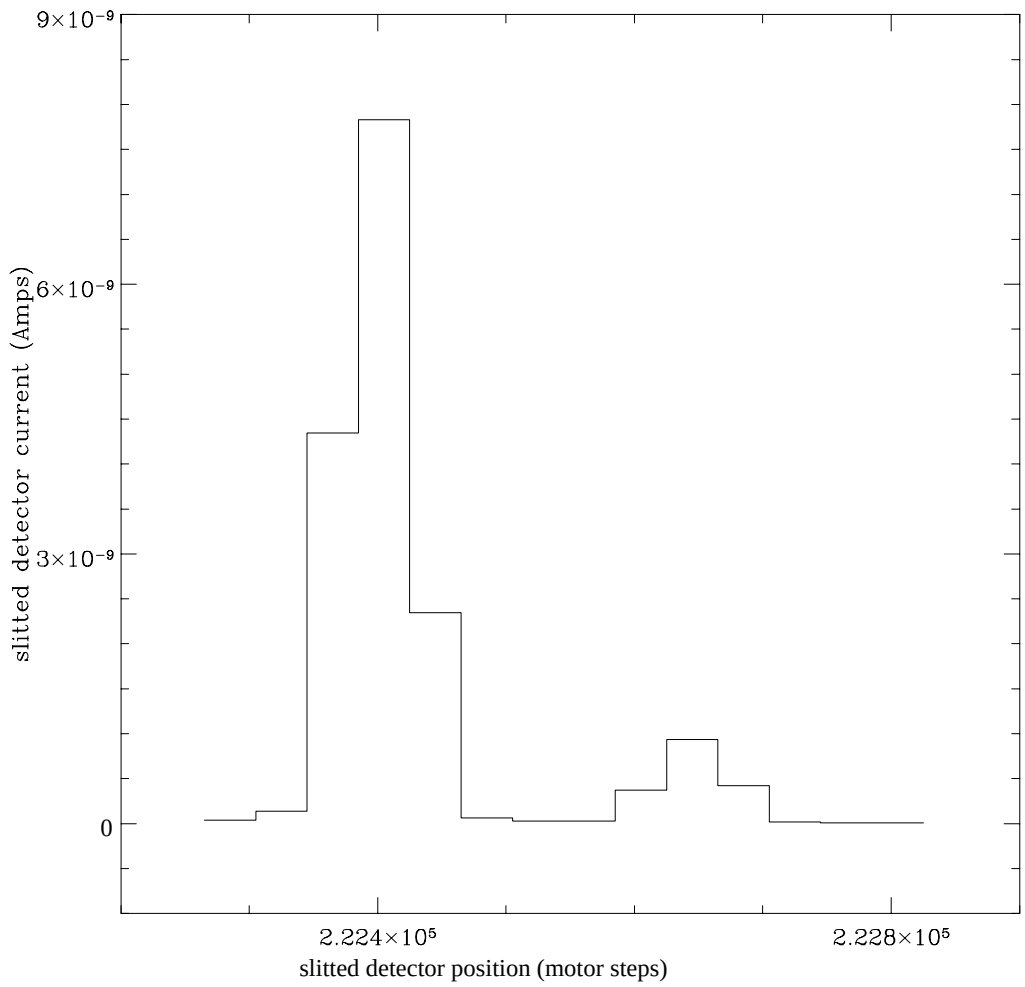

Figure 4-9: 2 mil slitted detector scan at 5.6 keV. Zeroth grating diffraction order on left and first grating diffraction order on right.

For the 0.708–2.025 keV energy range, the slitted detector current to monitor detector current ratios were then fit with a triple Gaussian function, which was the function found to have the best fit to the data. The Gaussian fits corresponded to the zeroth and first order as well as a reflection of the first order about the center of the zeroth order (to allow for the tail of the -1^{st} order). The parameters from the fits were used to integrate over the orders and obtain preliminary, un-normalized efficiencies. These efficiencies were normalized by dividing by the 2 mil slitted detector calibration scan results.

For the 4.0–6.6 keV energy range, no reasonable fits could be made to the data. So the slitted detector current to monitor detector current ratios were summed up over the zeroth and first grating diffraction orders. The limits used for the summation at 4.4 keV are shown as the solid lines in Figure 4-10. As can be seen in the figure, the lack of fitting the data seems reasonable because of the absence of tails on the diffraction orders. The current ratio sums were the preliminary, un-normalized efficiencies in this energy range. The normalization was carried out by dividing these efficiencies by the second order polynomial (shown earlier in Figure 4-6), which was a fit to the 2 mil slitted detector calibration data.

A common source of uncertainty in the normalized efficiencies was variation in the slitted detector background. As a measurement of this, the rms deviation of the background was calculated and divided by the average monitor detector reading to determine an uncertainty in the normalized efficiencies. Energies that were set with the silicon monochromator had an additional uncertainty due to the extrapolation of the slitted detector calibration to energies at which no calibration data was collected. To measure this uncertainty, the rms deviation of the calibration data from the second order polynomial fit for the 2.03–4.2 keV energy range and also for the 4.0–6.6 keV energy range was measured (see Figures 4-4 and 4-6). This resulted in an uncertainty in the normalization, which was propagated into the efficiency measurements. Energies that were set with the multi-layer monochromator did not have this additional uncertainty because calibration scans were conducted at every energy for which there was grating efficiency data.

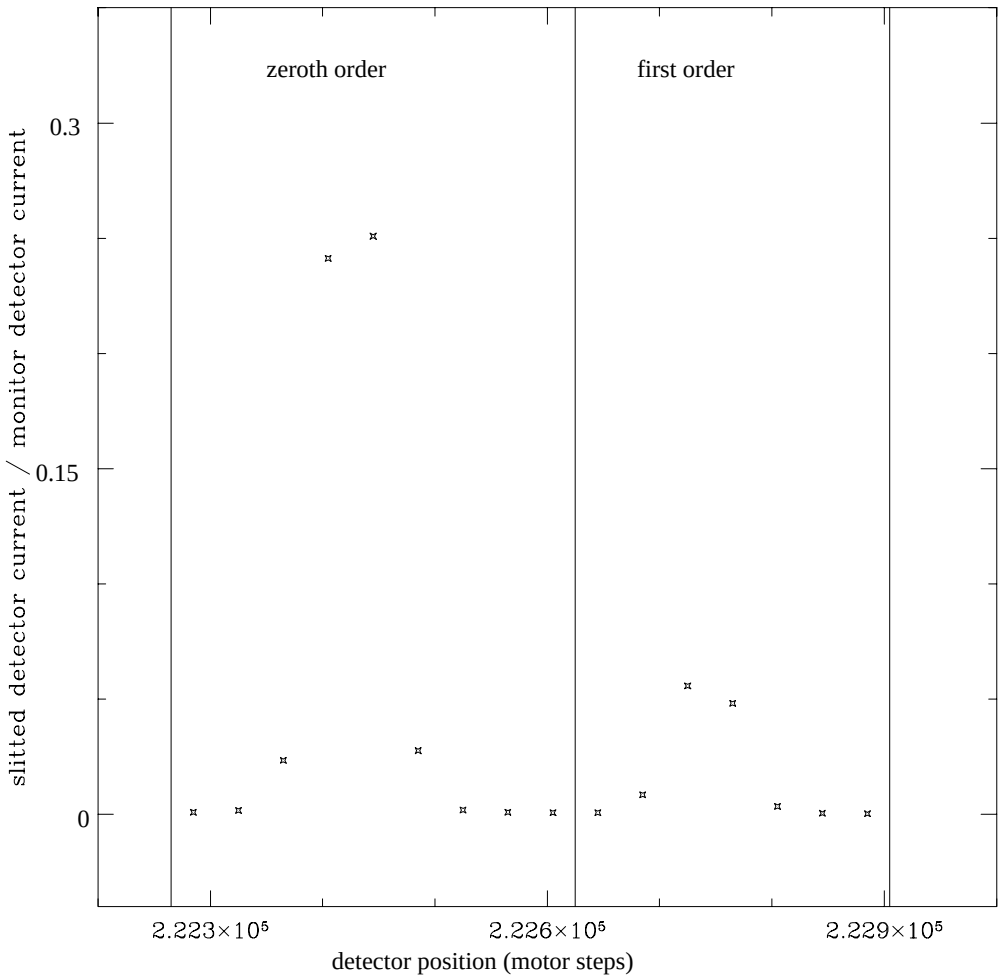

Figure 4-10: 2 mil slitted detector scan at 4.4 keV along with limits used for calculating zeroth and first order efficiency (vertical lines). Zeroth grating diffraction order on left and first grating diffraction order on right.

An additional source of uncertainty in the normalized efficiencies due to the fact that the slitted detector and monitor detector readings were not made simultaneously was investigated. We found that given the stability of the beam and the short amount of time between the slitted detector and monitor detector readings, this is an insignificant error (5–6 orders of magnitude smaller than the uncertainty due to the rms deviation of the detector background) and can safely be ignored.

The final efficiencies and uncertainties of all three energy ranges are shown below for zeroth order (Figure 4-11) and for first order (Figure 4-12). Note that the first order efficiencies include both first orders (which is assumed to be twice the measured, positive, first order). The efficiencies in the two figures are tabulated in Appendix A.

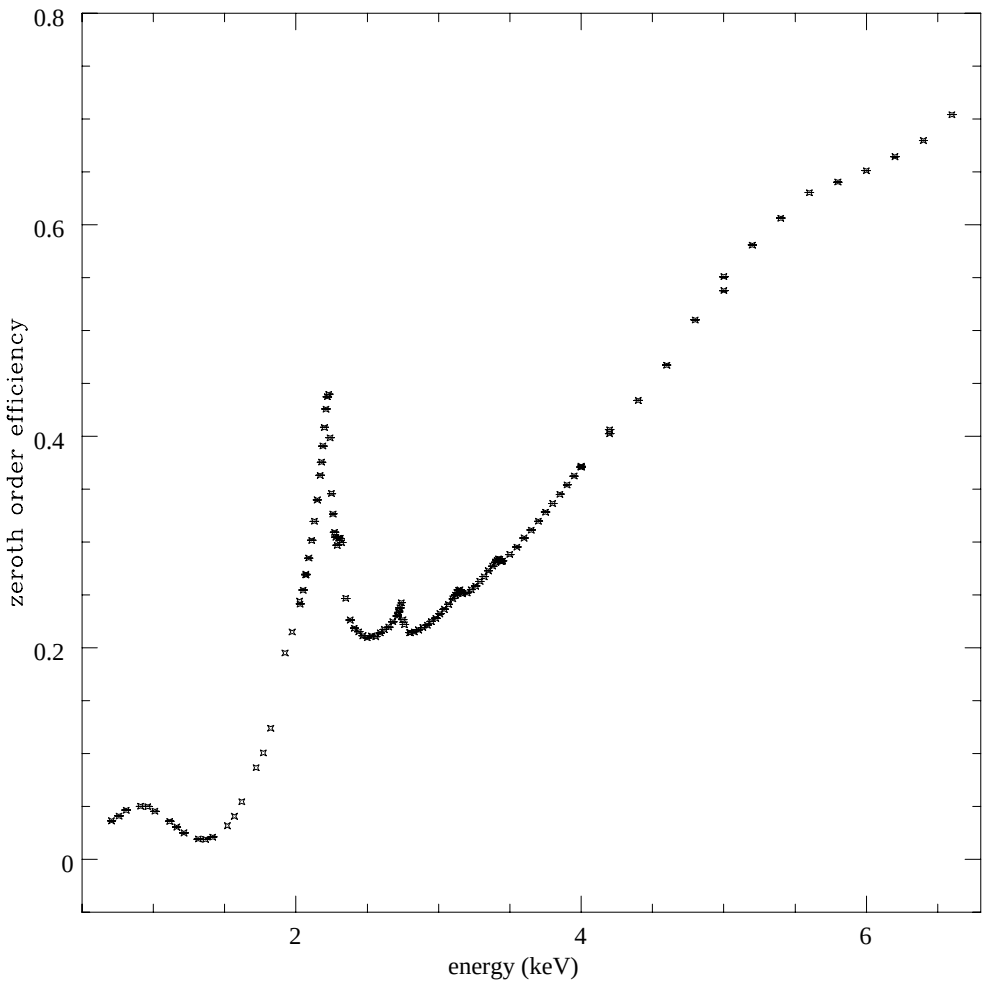

Figure 4-11: Zeroth order efficiency.

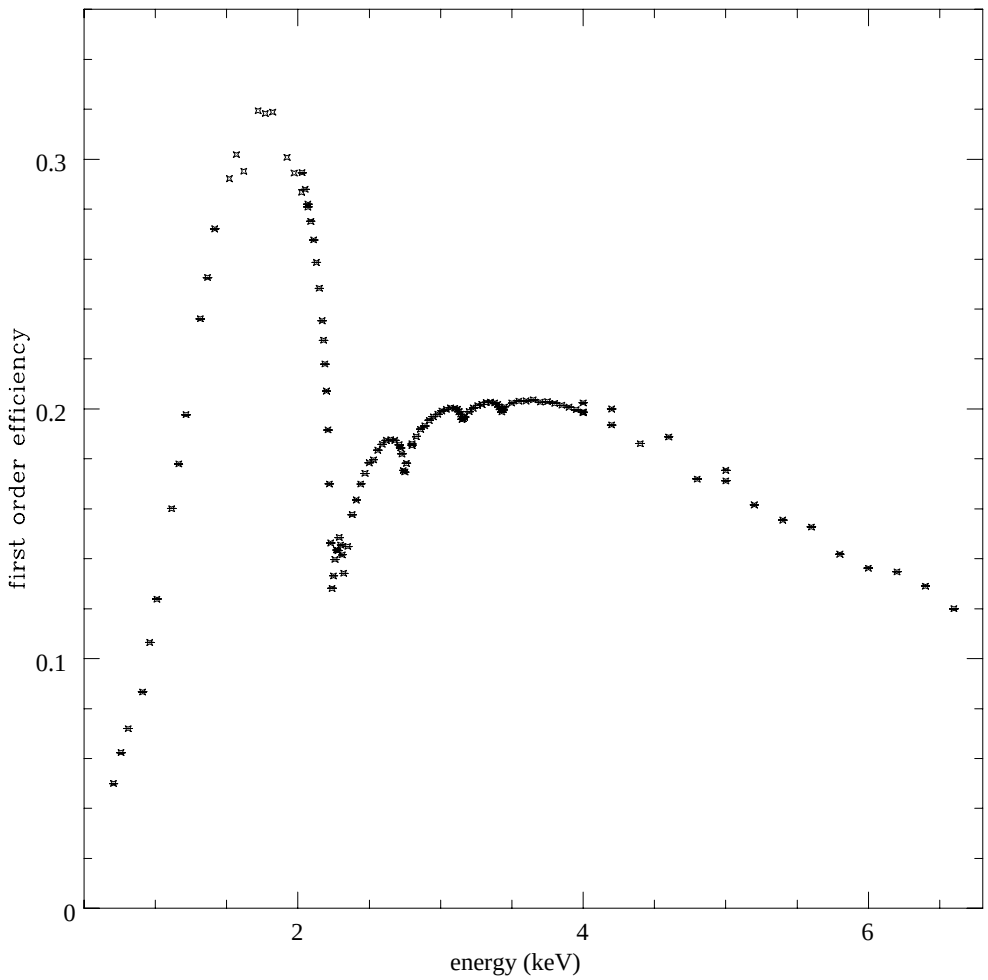

Figure 4-12: First order efficiency.

Chapter 5

Understanding the National Synchrotron Light Source Results

The program XRAY is the primary tool used to evaluate theoretical grating efficiencies in this thesis. XRAY was written by Mark Schattenburg and is a simplification of the complex diffraction theory in which the polarization of incident radiation is ignored. The equation used by XRAY that governs grating efficiency was discussed earlier in Section 2.3 (equation 2.7). The optical constants used by XRAY are from the July 1992 Henke tables (Henke *et al.*, 1993).

5.1 Theoretical Model with Standard Parameters vs. Data

Using the nominal parameters listed in Table 3.1 as well as the thicknesses of plating base materials and polyimide support structure shown in Table 5.1 below (Schattenburg, 1994, private communication) and a tilt from normal incidence of 0.15 degrees, I calculated the curve in Figure 5.1 using XRAY. The measured first order efficiencies are also shown as points on the figure. Note that the data and theory are in fairly good agreement (never more than 8% deviation). Yet since our goal is to calibrate the efficiencies to the 1% level, it would be better if the theory and data were to agree

Table 5.1: Plating base material and support structure thicknesses used for calculating the theoretical efficiencies (Schattenburg, 1994, private communication).

gold	200 Å ± 20 Å
chromium	10 Å ± 1 Å
nickel	40 Å ± 4 Å
polyimide support structure	1.0 ± 0.1 μm

that that level of accuracy. What follows is a discussion of the energy regions where disagreement is observed. Section 5.2 continues with a discussion of the possible sources of disagreement that my colleagues and I are investigating.

One of the more easily explained sources of disagreement between the theory and the data has to do with the location of the sharp dip in efficiency at about 2200 eV. The dip at this energy is due to the gold MV edge, which was reported by Henke *et al.*, 1993, to be at 2206 eV. More recent experiments conducted by Blake *et al.*, in press, have located the MV edge at 2247 ± 5 eV. This ∼40 eV shift is what is also observed between the theory and data of Figure 5-1.

Another source of disagreement between the theory and the data is the lower efficiency of the theory in the high energy ($\geq$ 4 keV) range (almost 8% deviation at 6.6 keV). Note that this energy range corresponds to the region in which we used a different method to obtain the efficiencies— that is, we mapped out the zeroth and first diffraction orders using a detector that had a 2 mil slit glued to its face. The significance of this fact will be discussed later (Section 5.3).

One possible source of the discrepancy in the 4 keV and higher energy range has to do with the thickness of one of the plating base materials— gold. Since the thickness of the gold has less of an effect on the efficiency for higher energies as it becomes more transparent, it might be possible to change the shape of the predicted efficiency curve in Figure 5-1 so that both the middle energy range (2–4 keV where the agreement is good) and the high energy range agree with the predicted efficiencies. This could involve shifting the entire theoretical efficiency curve upward (say, by decreasing the

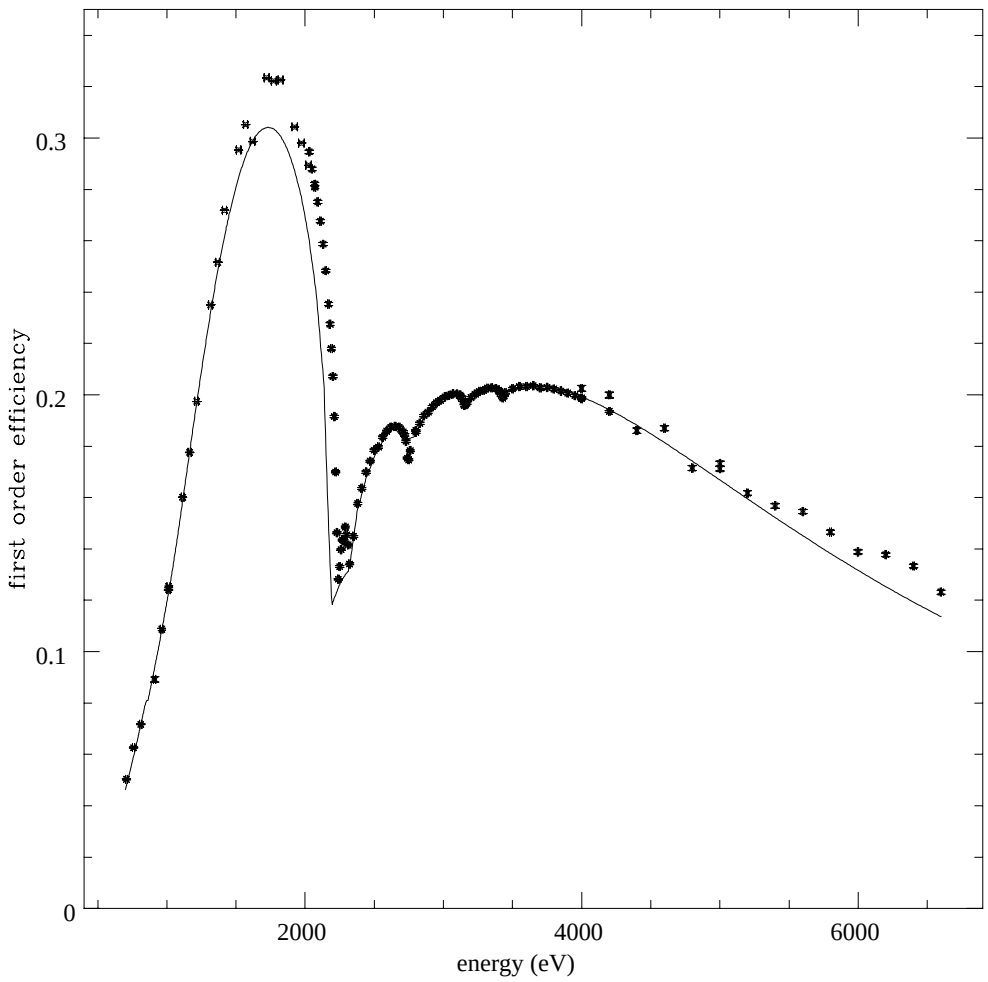

Figure 5-1: Theoretical and measured first order efficiencies. The theoretical efficiencies were calculated using XRAY.

bar width to period ratio) and then increasing the thickness of the gold in the plating base. The thickness could be chosen to shift the efficiency curve downward to exactly agree with the data in the 2–4 keV energy range, but since gold in the plating base has less of an effect for high energies, this region of the theoretical efficiencies would be closer to the measured values. An attempt to get better agreement between model and data by varying the nominal gold thickness (and other parameters) are discussed below (Section 5.2).

The most significant deviation between the theory and the data occurs at the peak in the efficiency between about 1500 and 2000 eV. The ~6% difference between the values cannot be explained away by uncertainties in plating base thicknesses since the deviation should be even larger at lower energies, where absorption is higher and yet we have agreement between the theoretical and measured efficiencies. Proposed sources of the discrepancy in the 1500–2000 eV energy range include uncertainties in the gold optical constants and the grating bar shape. The grating bar shape has been proposed because of the observation of trapezoidal bar shapes from SEM pictures of gratings. XRAY is capable of using trapezoidal bar shapes, but so far we have been assuming a rectangular bar shape as the nominal bar shape. In the next section, efficiency parameter variation is explored in an attempt to understand the deviations in Figure 5-1.

5.2 Parameter Variation

Given the number of efficiency measurements made at the synchrotron and the small uncertainty in those measurements as well as the relatively large uncertainty in many of the efficiency parameters, it may actually become more effective in the future to use our efficiency measurements to fit the parameters used by XRAY. But until we have confidence in the overall model and until the repeatability of our measurements can be tested, it is probably a better idea to investigate the variation of individual parameters so that we can learn more about their effects on the predicted efficiencies. What follows is a discussion of the role played by each parameter used by XRAY

(plating base thicknesses, polyimide thickness, grating bar shape, grating bar height, grating bar width to period ratio, and gold optical constants) in calculating the HX101 efficiencies.

Variation in the thickness of the chromium in the plating base is ineffective at reducing the deviation between the measured and theoretical efficiencies because it is virtually transparent at energies of 0.7 keV and higher. In fact, the transmission of 10 Å of chromium is almost 99% at 0.7 keV and increases exponentially for higher energies. The nickel in the plating base, on the other hand, is thicker than the chromium and also has an edge at 0.85 keV which reduces the transparency from over 99% to about 95%. The transparency then increases exponentially for higher energies. In any event, since the energy range affected by the plating base materials is not a region where deviation between the measured and theoretical efficiencies is observed, variation of these two parameters is not useful for our purposes.

Variation in the thickness of the gold in the plating base results in a shift of the theoretical efficiencies, which is independent of energy for energies less than about 4.5 keV[1]. A reasonable estimate of the uncertainty in the thickness of the gold in the plating base is ±10%— or 20 Å(Schattenburg, 1994, private communication). To see the effect of an uncertainty of this size, theoretical efficiencies for the nominal parameters and gold thicknesses of 180 Å and 220 Å are shown below in Figure 5-2. It is apparent from the figure that variation of the gold thickness will affect the ∼1.7 keV peak and the middle energy range (2–3.5 keV) roughly equally. Therefore, the use of a thinner gold layer will reduce the discrepancy at ∼1.7 keV, but it will create a new discrepancy in the middle energy range where we see agreement between the measured and theoretical efficiencies calculated using nominal values.

The transparency of the polyimide film increases exponentially from 37% at 0.7 keV to greater than 90% for energies above 1.6 keV, for the nominal 1 μm thickness. A reasonable uncertainty on the polyimide thickness is about 10% (Schattenburg, 1994, private communication). This corresponds to a maximum uncertainty in the

[1]The location of the gold edges does not matter because the grating bars are made of gold and therefore have edges at the same locations.

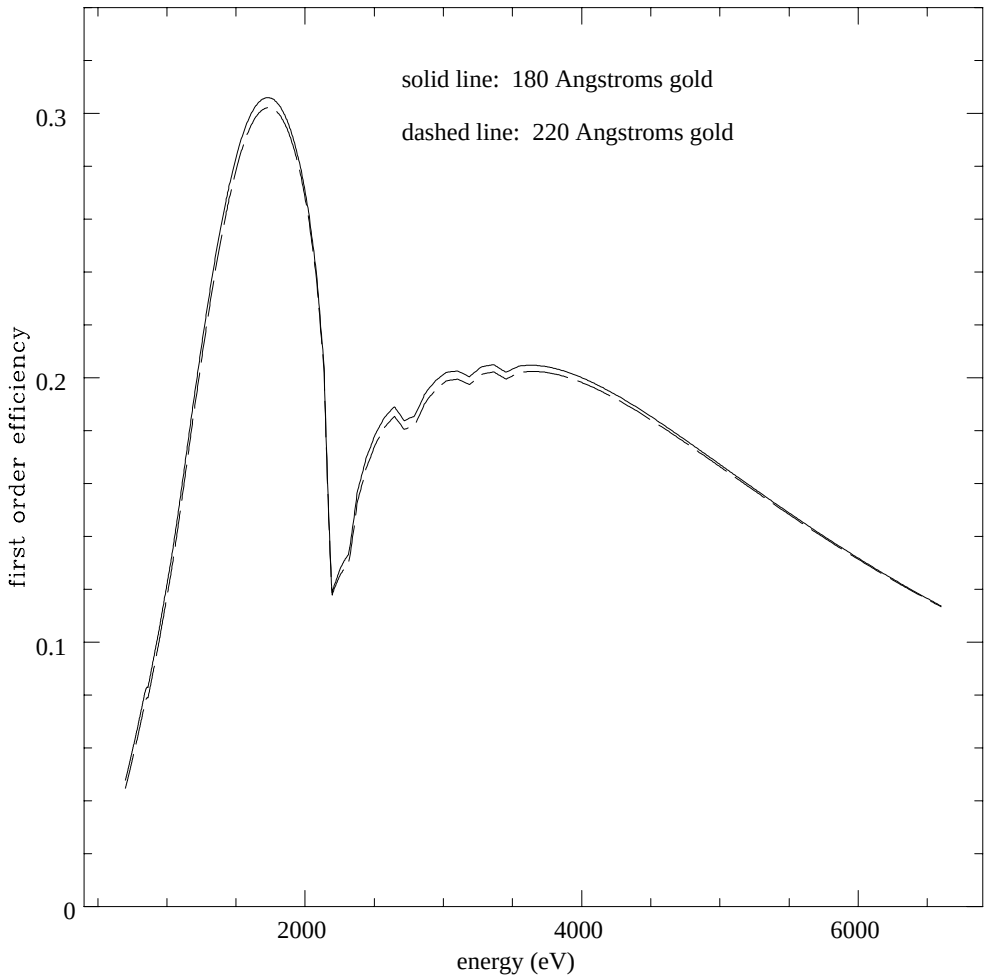

Figure 5-2: Effect of variation in the thickness of the gold in the plating base. The upper solid line corresponds to a 180 Å layer and the lower dashed line corresponds to a 220 Å layer.

transparency of $\pm 4\%$ at 0.7 keV, with smaller uncertainties in the transparency for higher energies. At the energy where we have the largest deviation between the measurements and the theory— about 1.7 keV— the uncertainty in the polyimide thickness results in an uncertainty in the transparency of less than $\pm 1\%$, which is significantly less than the $\sim 6\%$ deviation observed. Even if the polyimide thickness could be decreased to explain the $\sim 6\%$ deviation at 1.7 keV, the increase in transparency would have even more of an effect at lower energies where our data already agrees with the theoretical prediction. So to summarize, uncertainty in the polyimide thickness has a significant effect at lower energies, but it is not nearly large enough to explain the observed deviation between the theory and the data at 1.7 keV.

The simplistic, rectangular grating bar shape assumed by XRAY is another parameter that would be useful to vary in order to reduce or eliminate the deviations between the measured and theoretical efficiencies. Testing such a variation was made possible by using a program written by Yun Song that allows an arbitrary bar shape to be used to calculate grating efficiencies. By comparing trapezoidal and rectangular bar shapes, we found that the bar shape has an energy dependence in terms of its effect on efficiency. Figure 5-3 below shows the energy dependence. For the figure, we calculated efficiencies over the energy range of 0.7–6.6 keV for a rectangular bar shape and a trapezoidal bar shape (with an angle of 87.1 degrees for the bar side that connects the top and bottom of the bar) with identical cross-sectional areas[2]. The figure shows the fractional difference between the rectangular bar efficiencies and the trapezoidal efficiencies. As can be seen in the figure, the use of a trapezoidal bar shape would significantly decrease the efficiencies below 1 keV and have nearly the same effect at 2 keV as in the 4–6.6 keV energy range.

A parameter that results essentially in a shift of the efficiency curve for all energies in the 0.7–6.6 keV energy range is the grating bar width to period ratio (see equations

[2]For the rectangular bar shape calculation, a bar height of 4000 Å and a bar width of 1250 Å was used. For the trapezoidal bar shape, the bar height was also 4000 Å and the width of the peak (i.e., the narrowest part) of the trapezoid was 1050 Å. The areas of the trapezoid and the rectangle are equal for these dimensions. Neither grating model included any support structure or plating base materials.

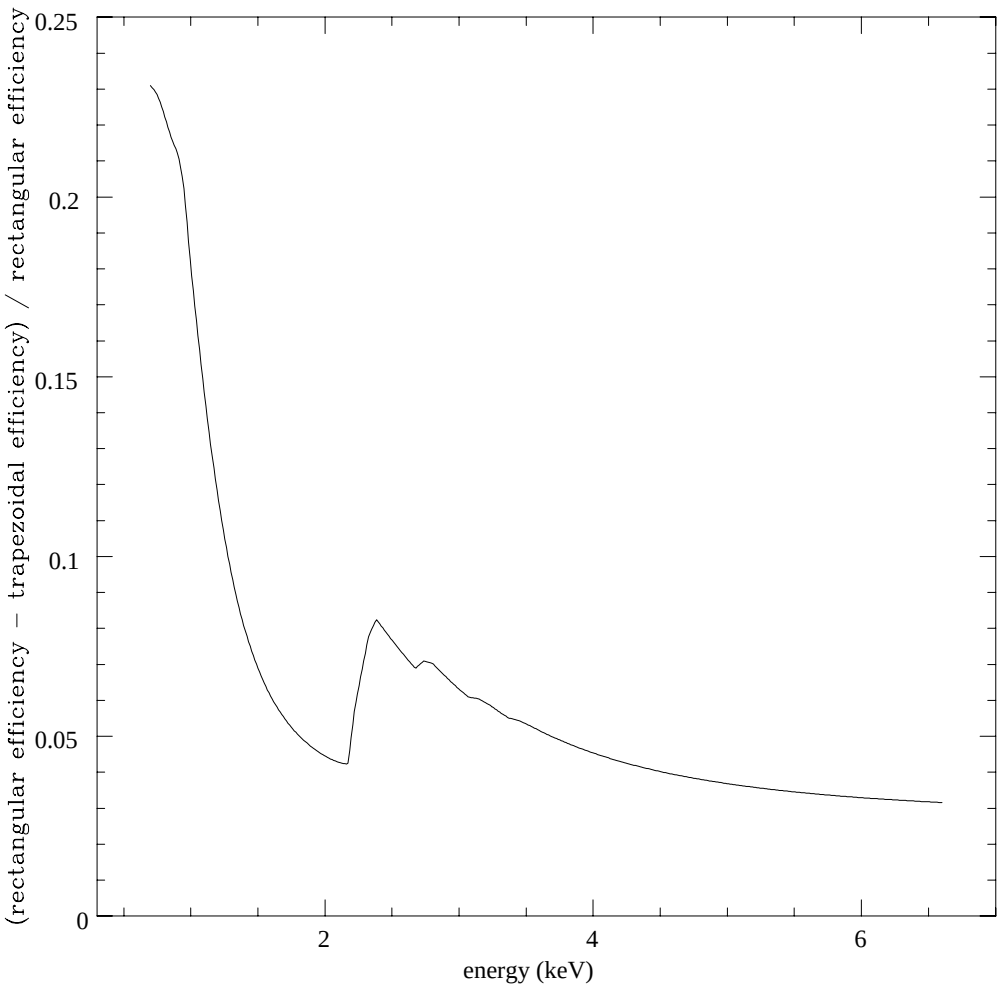

Figure 5-3: Fractional difference between efficiencies calculated using a rectangular bar shape and a trapezoidal bar shape. The dimensions of the trapezoid are such that the trapezoid and the rectangle have equal areas. The difference plotted is the rectangular efficiency minus the trapezoidal efficiency divided by the rectangular efficiency, as a function of energy.

2.6 and 2.7). The efficiencies are also very sensitive to this parameter (i.e. small changes in this parameter result in large changes in computed efficiencies). The uncertainty on the nominal ratio for HX101 is $\pm 2.1\%$ (Abdali *et al.*, 1993). To see the effect of a variation of this size in the ratio, Figure 5-4 below shows efficiency curves for $+\sigma$ and $-\sigma$. The natural conclusion that can be made based on Figure 5-4 is that while the grating bar width to period ratio has a significant effect on the efficiencies, it cannot (by itself) explain the energy dependence of the disagreement between the measured and theoretical efficiencies.

The optical constants not only have the gold M edges at incorrect energies, they also may be incorrect in their absolute values— especially near the absorption edges. One source of the uncertainty in the optical constants is the method used to calculate the real part of the index of refraction (i.e., the part that affects the phase shift). The imaginary part is directly related to the linear absorption coefficient, so it can be measured using transmission (assuming the density of the absorber is independently known). The real part, though, is not measured— it is calculated using the Kramers-Kronig relation (Schattenburg, 1982). The Kramers-Kronig relation involves an integral that can result in an incorrect value at energies where the imaginary part of the index of refraction changes quickly (i.e., near the absorption edges). We look forward to using updated values for the gold optical constants from the Blake *et al.* measurements, but as of this writing we must use the only constants available— those from the Henke tables.

Using the types of parameter variation described above in this Section, we were able to obtain a best-fit (by eye) theoretical model to the data. The model, which was created by XRAY, is shown below in Figure 5-5 and the parameters are listed in Table 5.2. The deviation at the 1.7 keV efficiency peak between the best-fit model and the data is 3.5%.

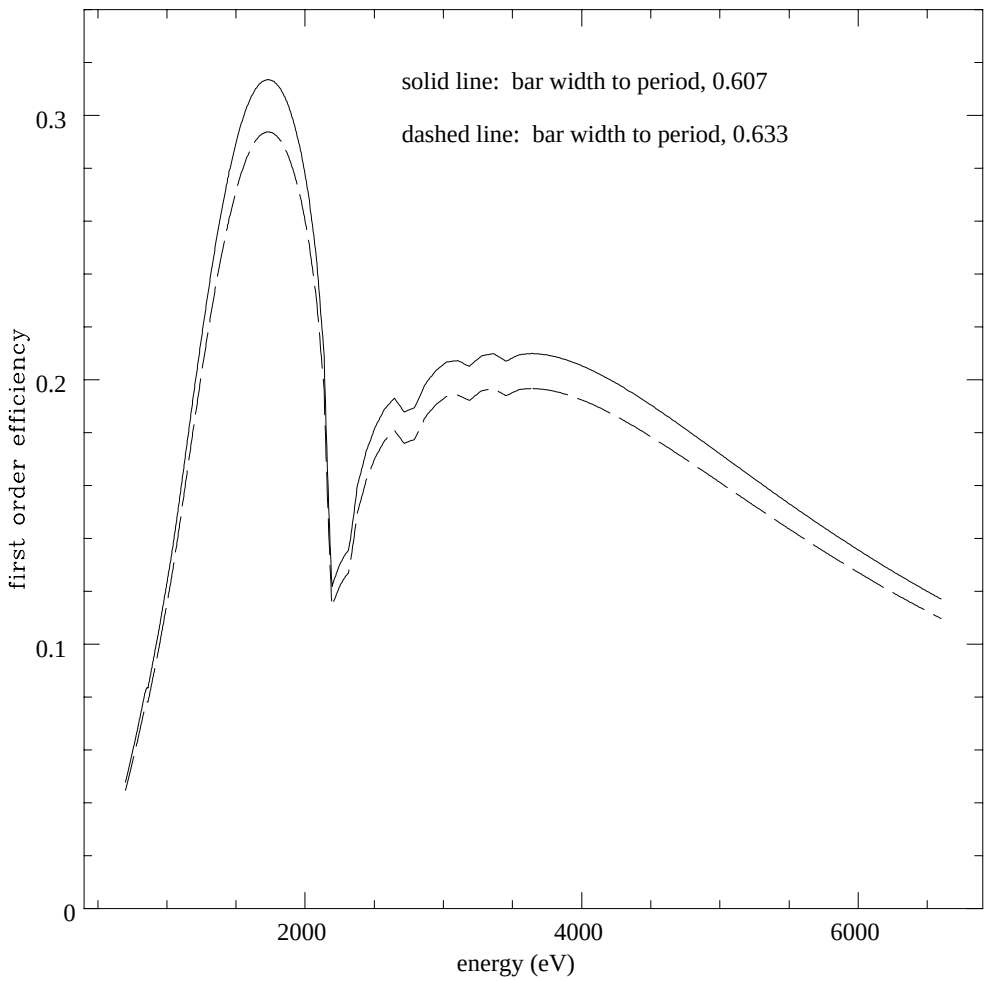

Figure 5-4: Effect of variation of the grating bar width to period ratio parameters on first order efficiency. The upper solid line corresponds to the nominal value minus σ and the lower dashed line corresponds to the nominal value plus σ.

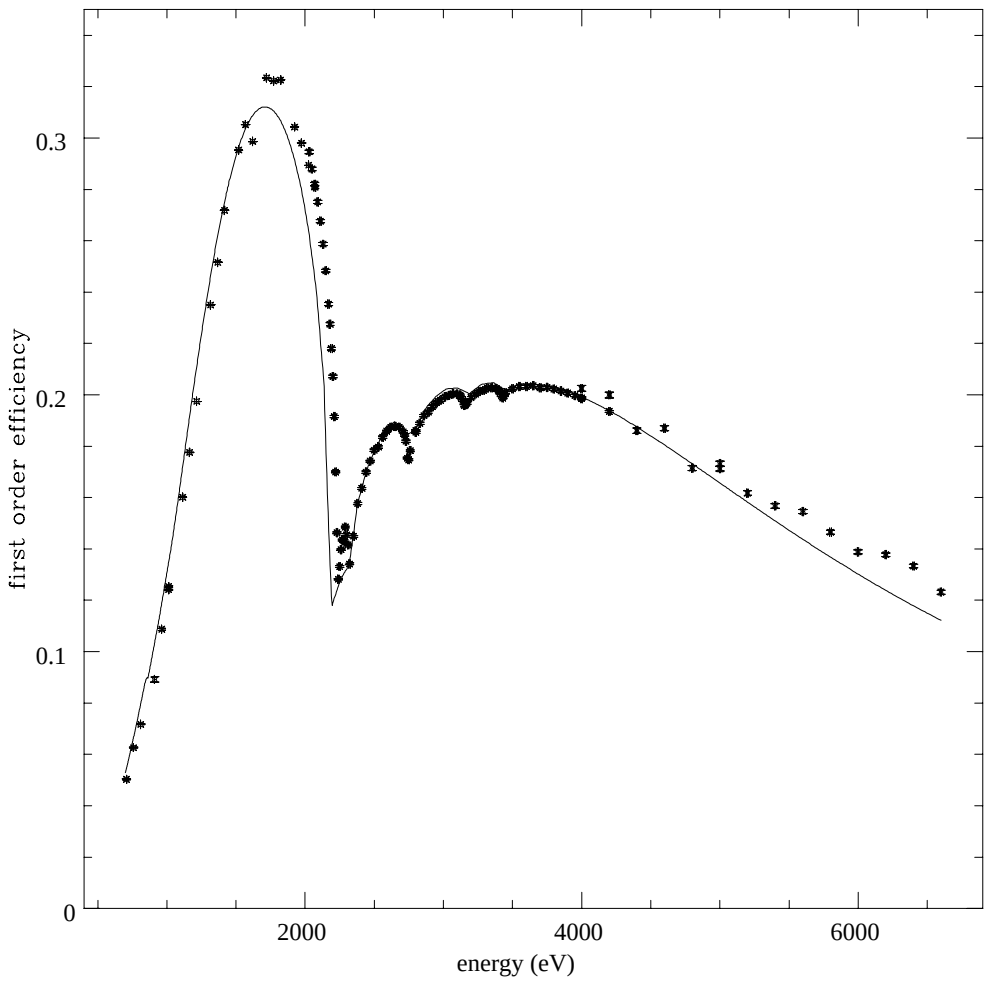

Figure 5-5: The best-fit theoretical model to the efficiency data. The parameters used by XRAY to create the model are listed in Table 5-2.

Table 5.2: Parameters used by XRAY to create the best-fit theoretical model to the efficiency data.

period	2001 Å
gap width	760 Å
bar height	3650 Å
top of bar width / bottom of bar width	0.95
gold	200 Å
chromium	10 Å
nickel	40 Å
polyimide support structure	0.9 μm

5.3 Conclusions on Theory/Data Discrepancy

Using the results of the last Section, we are left with two types of grating efficiency parameters— those that have little effect at any energy and those that affect both the ~1.7 keV peak and the middle energy range (2–3.5 keV) equally. With these two classes of parameters, we are unable to sufficiently reduce the ~1.7 keV discrepancy without creating a discrepancy in the middle energy range. One alternate proposal for overcoming this dilemma involves using the complex theory of diffraction.

The theory used by XRAY to calculate efficiencies, as mentioned earlier, ignores the vector nature of the incident radiation. In order to see the effect of this vector nature, Yun Song modified a program originally written by Erik Anderson (Anderson, 1988) that calculates grating efficiency using the complex diffraction theory. Figure 5-6 below is a comparison of the scalar and vector models used in the two different programs. As can be seen in the figure, the only energy for which the vector nature seems to make a difference is at the peak around 1.7 keV. There, the deviation between the two models is 1.5%. This is useful in that it reduces the 6% gap between the theory and the data, but it does not go far enough. There remains an unidentified source(s) that is contributing to the remaining 4.5% deviation.

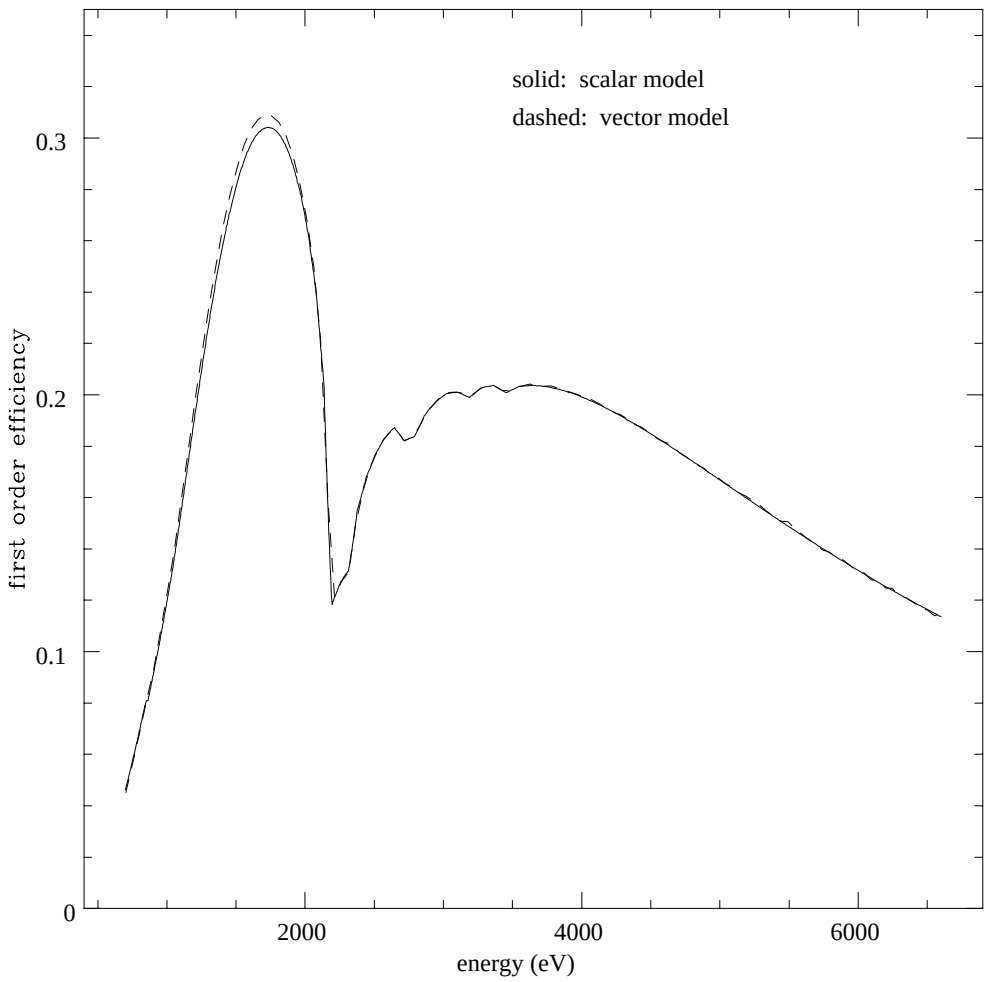

Figure 5-6: Scalar theory vs. vector theory for HX101 efficiency. The solid line corresponds to the scalar theory and the dashed line corresponds to the vector theory.

Another discrepancy that we are unable to explain is the higher measured efficiencies in the 4–6.6 keV energy range. It should be noted that we conducted two, double measurements at 4.0 keV and 4.2 keV, in which both methods of obtaining efficiencies— mapping with a 2 mil slitted detector and entire order detection with an 8 mil slitted detector— were used. Both of the measurements made using the 2 mil slitted detector were greater than those made using the 8 mil slitted detector. The 4.0 keV measurement was slightly more than 3σ's higher than the measurement made using the 8 mil slitted detector and the 4.2 keV measurement was almost 6σ's higher than the 8 mil slitted detector measurement. It is tempting to conclude from these double measurements and our inability to alter grating parameters such that they increase the efficiency in the 4–6.6 keV energy range that these higher measured efficiencies have some sort of systematic error due to the method used to obtain them. What that error may be remains unexplained. To avoid this type of error in the future, it would be better to use an alternate method of measuring the efficiencies in the high energy range (see Chapter 6).

Chapter 6

Conclusions on the National Synchrotron Light Source Tests

This Chapter is an opportunity to summarize the progress made in HETGS efficiency calibration as well as to comment on the future calibration plans. In January 1994, we (Markert, Graessle, Song, Flanagan, Bauer, and myself) submitted a general user proposal to the NSLS User Administrator requesting blocks of time on beam line X8A (the same beam line as was used for our previous two test runs) over the next two years. Our proposal was favorably reviewed and we have been given the period of June 2–13, 1994, as our first opportunity to conduct further experiments. Section 6.2 includes a preliminary test plan for this next round of efficiency tests.

6.1 Progress Toward Goals

The goals of the NSLS tests, which were discussed in Section 4.1, were a measurement of HX101 grating efficiency to 1%, the development of a better theoretical model based on the efficiency results, and progress toward an ultimate goal of producing calibration test standards. What follows is a discussion about the progress made in meeting these three goals.

The first of these goals— the measurement of efficiency to 1%— was accomplished over at least the 2.03–4 keV energy range. In fact, in this energy range, the uncertain-

ty in the first order efficiencies is ∼0.2% (see Appendix A). We can also be reasonably certain that there is no systematic error that we are ignoring in this energy range because the measurements of efficiency were so simple. That is, they involved comparing a single slitted detector measurement to a single monitor detector measurement and using the results of a straightforward detector cross-calibration to normalize the ratio of the two measurements.

For the high energy range (4–6.6 keV), the accomplishment of the 1% goal will have to await further tests. Although the formal uncertainties in the efficiencies in this energy range are all about 0.5–0.6% (see Appendix A), there is a suspected systematic error. The basis of this suspicion is both the observed scatter of the points around any sort of smooth curve as well as the double measurements that we conducted at 4 keV and 4.2 keV (see Section 5.3) in which the measurements made using the mapping technique with the 2 mil slitted detector were significantly greater than the measurements made using the 8 mil slitted detector.

In the low energy range (0.708–2.025 keV), whether or not the 1% goal was accomplished remains unclear. To begin with, the formal uncertainties in the efficiencies in this energy range are all under 1% (see Appendix A), except for one measurement at 0.911 keV where the uncertainty is 1.1%. A systematic error of the kind described in the section above cannot be proven on the basis of the double measurement of sorts that was conducted for the high end of this lower energy range, but neither can it be ruled out. This double measurement consisted of a measurement made using the 2 mil slitted detector at 2.025 keV and one using the 8 mil slitted detector at 2.03 keV. Although the energies of the two tests are essentially identical, it is misleading to compare a data point obtained with the multi-layer monochromator with a point obtained with the silicon monochromator. As mentioned in Chapter 4, the multi-layer crystals have an energy resolution of ∼50. At 2.025 keV, this means that the grating is looking at an energy range of the incident radiation of ∼2.005–2.045 keV. The efficiency we obtain is essentially an integration over this energy range where the contribution from different energies can be modelled as a Gaussian with a peak at 2.025 keV and a standard deviation of 17.20 eV (full width at half maximum,

40.50 eV, divided by 2.354). Computer simulations suggest that the value obtained by such an integration will be lower than the efficiency at 2.025 keV. This is what is also observed in our double measurement— the 2.03 keV efficiency is higher than the 2.025 keV efficiency.

To determine whether or not the 1% goal was met in the 0.708–2.025 keV energy range, we must also discuss the second goal— the development of a better theoretical model. As was summarized in Section 5.3, our attempts at improving the theoretical model with the use of parameter variation left one major unexplained discrepancy— the high measured efficiencies around 1.7 keV. Even the use of the complex diffraction theory, though helpful in reducing the discrepancy, did not eliminate it. So, the result is that the fulfillment of the 1% goal in the 0.708–2.025 keV energy range means that our second goal has not been fulfilled, or vice versa. More tests are clearly called for.

From the preceding discussion, it is clear that there are obstacles to overcome before an ultimate goal of making calibration test standards can be met. That leads to a discussion of the future test plans, which is the subject of the next Section.

6.2 Future Plans

The problem energy ranges for the January NSLS tests are the two in which the 2 mil slitted detector was used to map out the grating diffraction orders. The obvious means of avoiding these sorts of problems in the June 1994 tests is to eliminate the use of the 2 mil slitted detector. For the high energy range, this should be simple. In the January 1994 tests, we were being conservative by not using the 8 mil slitted detector at energies above 4.2 keV. For the constant dispersion distance of the test chamber and a narrower, 6.5 mil slitted detector, the 2000 Å period, grating diffraction orders are separated by greater than 6.5 mils for energies up to 6.6 keV. The only other requirement is that the beam must be narrower than the 6.5 mil slit— which we were able to accomplish in January when we used a 5 mil wide beam. To be conservative, an even narrower beam (say 4 mils) would be desirable.

For the lower energy range, eliminating the use of the 2 mil slitted detector is

more complicated. It would mean that we could not use the multi-layer crystals as monochromators because of their low resolution. The only other crystal pair that beam line X8A is equipped with and is also compatible for setting energies in the 0.8–2 keV energy range is a pair of beryl crystals with resolution ($E/\Delta E$) of 1250. The resolution of these crystals is adequate to prevent orders from overlapping, but we would have to worry about higher crystal order contamination. Disentangling crystal and diffraction orders can become messy, unless one has a particular piece of information— the crystal's efficiency at different orders, as a function of energy. This information could be easily obtained using a proportional counter on beam line X8A.

Given the length of the time we have been given on beam line X8A, we should be able to test several gratings. At the risk of seeming repetitive, one of those gratings should be HX101— this would allow us to check repeatability of the 2.03–4 keV measurements and remove our doubts about the low and high energy efficiency measurements. Additional gratings could be a flight-like HEG grating (if available) and an MEG grating. For all three gratings, the preliminary procedures at X8A will be identical— grating tilt tests for alignment purposes and detector cross-calibration over the entire energy range that will be studied. One modification to the January tests is that we should cross-calibrate the detector at every energy for which there will be a grating efficiency measurement so that we will not have to introduce into our efficiency measurements an additional error due to extrapolation from a fitted curve. The procedure for testing each of the three above-mentioned gratings will now be discussed.

6.2.1 HX101 re-testing

Since the 2.03–4 keV energy range of HX101 was studied so in-depth in January, we should just plan to verify the January measurements at a few energies (especially the lower energies— see below) before moving on to the problem energy ranges $<$ 2.03 keV and $>$ 4 keV. Of course, if the efficiencies cannot be verified, we should remain flexible in our test plan and spend more time investigating the source of any appreciable drift in efficiencies. There is also some interest in studying the energies

near the gold MV edge in detail— such as test intervals around 1 eV. These tests would allow us to look for fine structure in the efficiencies due to fine structure in the optical constants, which has recently been observed by Richard Blake (Blake, 1994, private communication).

In the 4–6.6 keV energy range, we could carry out efficiency measurements in 100 eV steps, a total of 27 tests. This should be sufficient given that the efficiency curve in this region should be smooth. In the lower energy range (0.8–2 keV)— assuming that we can use the beryl crystals and know their efficiency for different orders as a function of energy— we should also plan tests in 100 eV steps with a higher concentration (say 30 eV steps) near the peak efficiency of 1.7 keV. Altogether, this results in about 20 tests in this energy range. Repeatability tests should also be conducted at several energies in both the > 4 keV and < 2.03 keV energy ranges.

The energy range of the beryl crystals of 0.8–2.8 keV will allow us to compare measurements made using energies set with both the silicon crystals and the beryl crystals. We should plan to do this at at least five different energies. These tests could serve as our energy calibration for the beryl crystals so we will not have to change filters and search for absorption edges.

During all of the HX101 tests, real-time analysis will be crucial in determining whether or not to proceed with the test plan. Given the straightforward measurement procedure in which only two measurements are needed (as well as the detector cross-calibration), this should not be a problem.

6.2.2 flight-like HEG testing

The theoretical first order efficiency— as calculated by XRAY— of a flight-like HEG grating (period 2000 Å, bar height 6000 Å, bar width 1000 Å, polyimide thickness 1 μm, standard thicknesses for plating base materials[1]) is shown below in Figure 6-1.

The energy ranges in which to concentrate efficiency tests for a flight quality grating are essentially the same as for HX101— near the gold edges and the peak

[1]Gratings with these parameters will probably be available at the time of the tests.

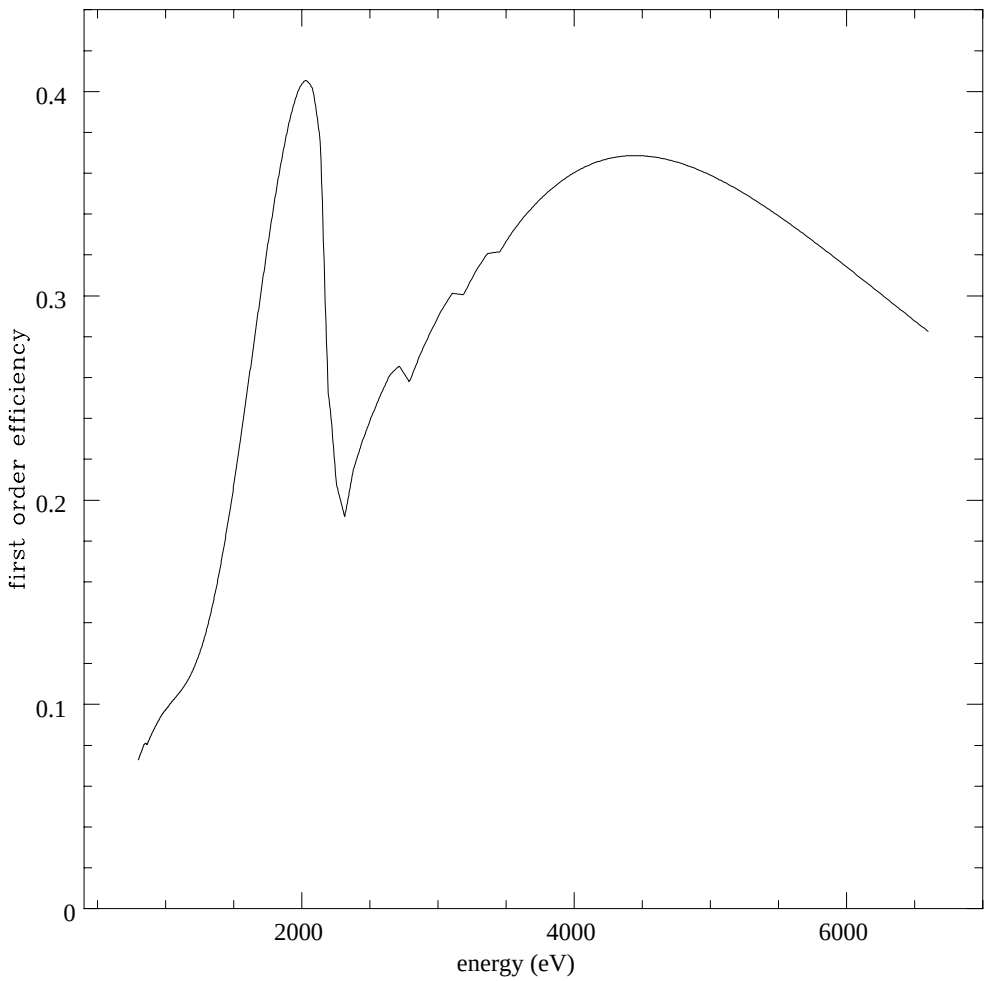

Figure 6-1: Theoretical first order efficiency for a flight-like HEG grating. Parameters used by XRAY include period 2000 Å, bar height 6000 Å, bar width 1000 Å, polyimide thickness 1 μm, and standard thicknesses for plating base materials.

from 1.7 keV up to the gold MV edge. A preliminary plan for the beryl crystal energy range would be to have tests every 100 eV from 0.8 keV up to 1.4 keV, then take measurements in 30 eV steps up to the lower edge of the silicon crystal energy range (2.03 keV). In the gold edge region (2.2–3.5 keV), tests would be conducted every 30 eV except near the edges where tests would be conducted in 10 eV intervals. At energies above the gold edges, tests would be conducted every 50 eV. Altogether, this adds up to about 150 tests. If time constraints become a problem, the high energy interval between tests could be increased to 100 eV. We should just be sure that we conduct enough tests to fully characterize the peak efficiency around 4.9 keV.

6.2.3 MEG testing

The theoretical first order efficiency— as calculated by XRAY— of an MEG grating (period 4000 Å, bar height 4000 Å, bar width 2000 Å, polyimide thickness 5000 Å, standard thicknesses for plating base materials) is shown below in Figure 6-2.

The similarity of the MEG theoretical efficiency to the HX101 theoretical efficiency is obvious from a glance at Figure 6-2. Because of this similarity, the HX101 energies studied in January could be repeated for the MEG. But since the MEG's have specifically been optimized for the lower energy end of the HETGS operating energy range, we should concentrate more efficiency tests in the 0.8–2.2 keV energy range. We could step through this energy range in 30 eV steps— for about 50 total tests. We should also make measurements at the higher energies, but we could step through in 100 eV intervals in the interest of time.

Because the HETGS operating energy range extends down to 0.4 keV, it would be useful to study the MEG's efficiency down to this energy. For tests in the 0.4–0.8 keV energy range, we must use the multi-layer crystals because this range is below the beryl crystals' energy range. We should plan to conduct efficiency tests every 50 eV in this energy range, and also repeat a few tests at energies in the beryl range. These duplicate tests can be used to normalize the multi-layer efficiencies and thereby eliminate the effects of a systematic error due to the mapping technique that must be used with multi-layer energies.

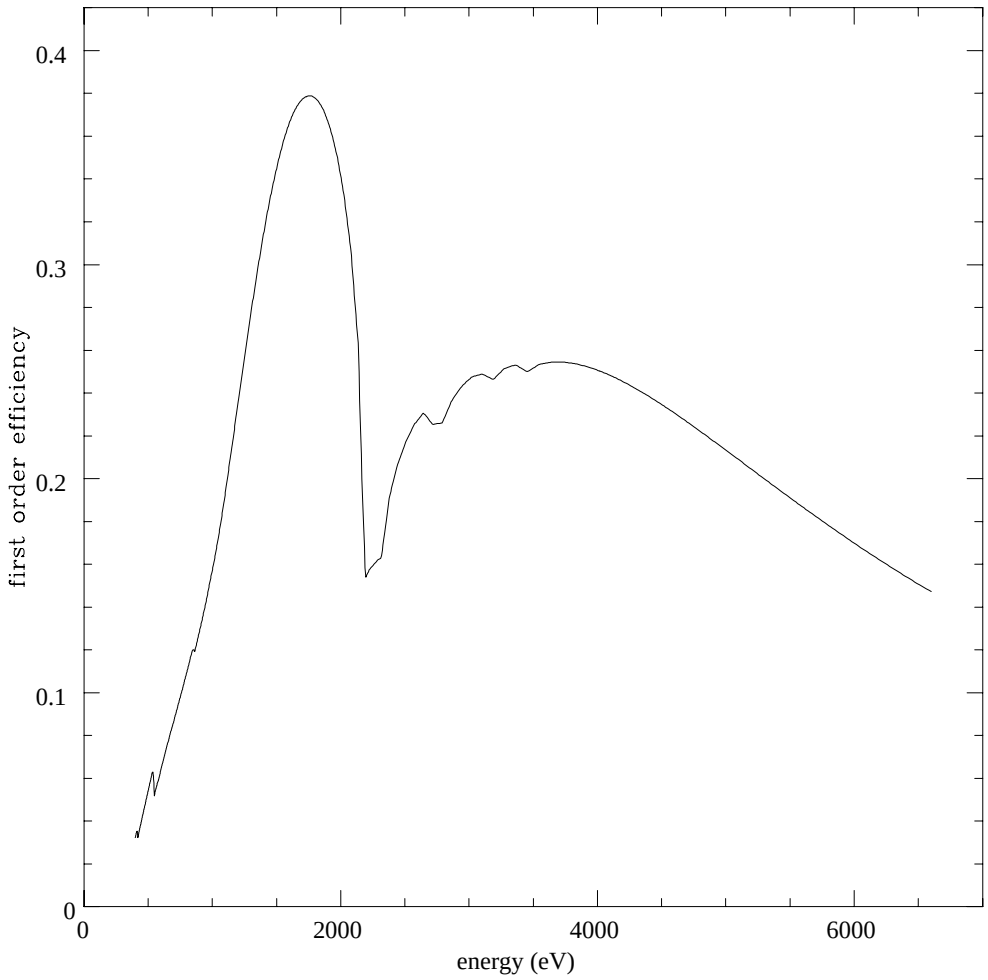

Figure 6-2: Theoretical first order efficiency for an MEG grating. Parameters used by XRAY include period 4000 Å, bar height 4000 Å, bar width 2000 Å, polyimide thickness 5000 Å, and standard thicknesses for plating base materials.

Appendix A

Efficiencies of HX101 in the energy range of 0.708–6.6 keV

The following Table lists the zeroth and first order efficiencies as measured at the NSLS in January 1994. See Chapter 4 for a discussion of how these values were calculated.

Table A.1: HX101 zeroth and first order efficiencies, as measured at the National Synchrotron Light Source in January 1994.

energy (keV)	zeroth order efficiency	first order efficiency
0.708 ± 0.007	0.03633 ± 0.00012	0.05030 ± 0.00025
0.759 ± 0.008	0.04148 ± 0.00010	0.06266 ± 0.00021
0.810 ± 0.008	0.050132 ± 0.000093	0.07171 ± 0.00019
0.911 ± 0.009	0.05013 ± 0.00050	0.08919 ± 0.00099
0.962 ± 0.010	0.05035 ± 0.00021	0.10874 ± 0.00042
1.012 ± 0.010	0.04609 ± 0.00011	0.12415 ± 0.00021
1.012 ± 0.010	0.04542 ± 0.00013	0.12534 ± 0.00026
1.114 ± 0.011	0.036201 ± 0.000055	0.16017 ± 0.00011
1.164 ± 0.012	0.030658 ± 0.000031	0.177579 ± 0.000063
1.215 ± 0.012	0.0249995 ± 0.0000053	0.197462 ± 0.000011
1.316 ± 0.013	0.0189903 ± 0.0000078	0.235042 ± 0.000016
1.367 ± 0.014	0.0188152 ± 0.0000052	0.251606 ± 0.000010
1.417 ± 0.014	0.0210044 ± 0.0000044	0.2718655 ± 0.0000089
1.519 ± 0.015	0.0322633 ± 0.0000021	0.2953591 ± 0.0000041
1.569 ± 0.016	0.0412354 ± 0.0000020	0.3052263 ± 0.0000040
1.620 ± 0.016	0.0552403 ± 0.0000015	0.2986425 ± 0.0000030
1.721 ± 0.017	0.0877337 ± 0.0000015	0.3234697 ± 0.0000030
1.772 ± 0.018	0.1019945 ± 0.0000019	0.3222072 ± 0.0000038
1.823 ± 0.018	0.1255366 ± 0.0000036	0.3226229 ± 0.0000073
1.924 ± 0.019	0.197560 ± 0.000011	0.304337 ± 0.000022
1.974 ± 0.020	0.2176380 ± 0.0000050	0.298043 ± 0.000010
2.025 ± 0.020	0.2464148 ± 0.0000052	0.289396 ± 0.000010
2.030 ± 0.005	0.24159 ± 0.00029	0.29465 ± 0.00070
2.050 ± 0.005	0.25468 ± 0.00029	0.28797 ± 0.00066

energy (keV, ± 0.005 keV)	zeroth order efficiency	first order efficiency
2.07	0.26917 ± 0.00032	0.28087 ± 0.00066
2.07	0.26979 ± 0.00032	0.28205 ± 0.00066
2.09	0.28498 ± 0.00033	0.27516 ± 0.00063
2.11	0.30177 ± 0.00034	0.26769 ± 0.00061
2.13	0.31980 ± 0.00037	0.25867 ± 0.00061
2.15	0.34003 ± 0.00039	0.24835 ± 0.00058
2.17	0.36323 ± 0.00042	0.23535 ± 0.00054
2.18	0.37576 ± 0.00043	0.22751 ± 0.00052
2.19	0.39094 ± 0.00044	0.21801 ± 0.00050
2.20	0.40846 ± 0.00047	0.20717 ± 0.00048
2.21	0.42592 ± 0.00049	0.19158 ± 0.00044
2.22	0.43765 ± 0.00050	0.16999 ± 0.00040
2.23	0.43980 ± 0.00050	0.14633 ± 0.00035
2.24	0.39874 ± 0.00045	0.12817 ± 0.00030
2.25	0.34611 ± 0.00040	0.13317 ± 0.00032
2.26	0.32666 ± 0.00037	0.13972 ± 0.00033
2.27	0.30937 ± 0.00035	0.14355 ± 0.00034
2.28	0.30475 ± 0.00035	0.14326 ± 0.00034
2.29	0.29706 ± 0.00034	0.14856 ± 0.00035
2.30	0.30387 ± 0.00035	0.14553 ± 0.00034
2.31	0.30375 ± 0.00035	0.14157 ± 0.00033
2.32	0.29960 ± 0.00034	0.13417 ± 0.00032
2.35	0.24693 ± 0.00028	0.14494 ± 0.00034
2.38	0.22641 ± 0.00026	0.15769 ± 0.00037
2.41	0.21868 ± 0.00025	0.16358 ± 0.00038
2.44	0.21534 ± 0.00024	0.16993 ± 0.00039
2.47	0.21163 ± 0.00024	0.17422 ± 0.00040

energy (keV, ± 0.005 keV)	zeroth order efficiency	first order efficiency
2.50	0.20955 ± 0.00024	0.17848 ± 0.00041
2.53	0.21131 ± 0.00024	0.17968 ± 0.00041
2.56	0.21069 ± 0.00024	0.18347 ± 0.00042
2.59	0.21420 ± 0.00024	0.18589 ± 0.00042
2.62	0.21750 ± 0.00025	0.18742 ± 0.00043
2.65	0.21980 ± 0.00025	0.18774 ± 0.00042
2.68	0.22480 ± 0.00025	0.18742 ± 0.00042
2.71	0.23023 ± 0.00026	0.18569 ± 0.00042
2.72	0.23384 ± 0.00026	0.18446 ± 0.00042
2.73	0.23790 ± 0.00027	0.18200 ± 0.00041
2.74	0.24276 ± 0.00027	0.17539 ± 0.00040
2.75	0.22676 ± 0.00026	0.17474 ± 0.00040
2.76	0.22207 ± 0.00025	0.17823 ± 0.00040
2.80	0.21441 ± 0.00024	0.18541 ± 0.00042
2.80	0.21458 ± 0.00024	0.18605 ± 0.00042
2.83	0.21526 ± 0.00024	0.18897 ± 0.00043
2.86	0.21712 ± 0.00024	0.19188 ± 0.00043
2.89	0.21940 ± 0.00025	0.19325 ± 0.00044
2.92	0.22171 ± 0.00025	0.19545 ± 0.00044
2.95	0.22508 ± 0.00025	0.19692 ± 0.00044
2.98	0.22809 ± 0.00026	0.19792 ± 0.00044
3.01	0.23234 ± 0.00026	0.19924 ± 0.00045
3.04	0.23657 ± 0.00026	0.19984 ± 0.00045
3.07	0.24117 ± 0.00027	0.20048 ± 0.00045
3.10	0.24657 ± 0.00028	0.20030 ± 0.00045
3.12	0.25012 ± 0.00028	0.19988 ± 0.00045

energy (keV, ± 0.005 keV)	zeroth order efficiency	first order efficiency
3.13	0.25232 ± 0.00028	0.19892 ± 0.00044
3.14	0.25443 ± 0.00028	0.19786 ± 0.00044
3.15	0.25480 ± 0.00028	0.19583 ± 0.00044
3.16	0.25192 ± 0.00028	0.19619 ± 0.00044
3.17	0.25132 ± 0.00028	0.19678 ± 0.00044
3.20	0.25207 ± 0.00028	0.19898 ± 0.00044
3.23	0.25516 ± 0.00028	0.20035 ± 0.00045
3.26	0.25850 ± 0.00029	0.20137 ± 0.00045
3.29	0.26296 ± 0.00029	0.20178 ± 0.00045
3.32	0.26736 ± 0.00030	0.20263 ± 0.00045
3.35	0.27304 ± 0.00030	0.20271 ± 0.00045
3.38	0.27744 ± 0.00031	0.20239 ± 0.00045
3.40	0.28110 ± 0.00031	0.20180 ± 0.00045
3.41	0.28284 ± 0.00032	0.20088 ± 0.00045
3.42	0.28434 ± 0.00032	0.19982 ± 0.00044
3.43	0.28376 ± 0.00032	0.19880 ± 0.00044
3.44	0.28171 ± 0.00031	0.19969 ± 0.00044
3.45	0.28224 ± 0.00031	0.20085 ± 0.00045
3.50	0.28839 ± 0.00032	0.20241 ± 0.00045
3.55	0.29545 ± 0.00033	0.20320 ± 0.00045
3.60	0.30394 ± 0.00034	0.20322 ± 0.00045
3.65	0.31152 ± 0.00035	0.20364 ± 0.00045
3.70	0.31986 ± 0.00036	0.20276 ± 0.00045
3.75	0.32842 ± 0.00036	0.20294 ± 0.00045
3.80	0.33663 ± 0.00037	0.20229 ± 0.00045
3.85	0.34532 ± 0.00038	0.20147 ± 0.00045

energy (keV, ± 0.005 keV)	zeroth order efficiency	first order efficiency
3.90	0.35418 ± 0.00039	0.20071 ± 0.00044
3.95	0.36263 ± 0.00040	0.19970 ± 0.00044
4.00	0.37103 ± 0.00041	0.19882 ± 0.00044
4.00	0.37105 ± 0.00041	0.19852 ± 0.00044
4.00	0.3718 ± 0.0010	0.2025 ± 0.0011
4.20	0.40635 ± 0.00045	0.19357 ± 0.00043
4.20	0.4027 ± 0.0011	0.2000 ± 0.0011
4.40	0.4341 ± 0.0012	0.1861 ± 0.0010
4.60	0.4668 ± 0.0013	0.1870 ± 0.0010
4.80	0.5095 ± 0.0014	0.17148 ± 0.00094
5.00	0.5512 ± 0.0015	0.17322 ± 0.00094
5.00	0.5380 ± 0.0015	0.17122 ± 0.00093
5.20	0.5835 ± 0.0016	0.16173 ± 0.00088
5.40	0.6115 ± 0.0017	0.15679 ± 0.00085
5.60	0.6382 ± 0.0017	0.15458 ± 0.00084
5.80	0.6507 ± 0.0018	0.14656 ± 0.00080
6.00	0.6650 ± 0.0018	0.13882 ± 0.00076
6.20	0.6805 ± 0.0018	0.13775 ± 0.00076
6.40	0.6984 ± 0.0019	0.13334 ± 0.00075
6.60	0.7232 ± 0.0020	0.12323 ± 0.00078

Bibliography

[1] *AXAF-I Level I Program Requirements Document.*

[2] Abdali, S., Christensen, F.E., Schnopper, H.W., Markert, T.H., Dewey, D., and Nelson, C.S. "High Resolution X-Ray Studies of an AXAF High Energy Transmission Grating", *Multilayer and Grazing Incidence X-Ray/EUV Optics II*, Proc. SPIE, Vol. 2011, July 1993.

[3] Anderson, E.H. "Fabrication and Electromagnetic Applications of Periodic Nanostructures", MIT Ph.D. thesis, 1988.

[4] Bevington, Philip R. *Data Reduction and Error Analysis for the Physical Sciences.* New York: McGraw-Hill, 1969.

[5] Blake, R.L., Davis, J.C., Graessle, D.E., Burbine, T.H., and Gullikson, E.M. "Optical Constants and Scattering Factors from Reflectivity Measurements: 50 eV to 5 keV", *Journal of X-ray Science and Technology*, in press.

[6] Born, Max, and Wolf, Emil. *Principles of Optics.* Oxford: Pergamom, 1970.

[7] Canizares, C.R., Dewey, D., Galton, E.B., Markert, T.H., Smith, H.I., Schattenburg, M.L., Woodgate, B.E., and Jordan, S. "The MIT High Resolution X-Ray Spectroscopy Instruments on AXAF", presented at the *AIAA Space Programs and Technologies Conference*, Huntsville, AL, March 1992.

[8] Canizares, C.R., and Kruper, J. "A Sharp X-ray Absorption Feature in the LB Lacertae Object PKS 2155-304", *Astrophysical Journal (Letters)*, Vol. 278, 1984.

[9] Ceglio, N.M. "Revolution in X-Ray Optics", *Journal of X-ray Science and Technology*, Vol. 1, July, 1989.

[10] Christensen, F.E., Hornstrup, A., Frederiksen, P., Abdali, S., Grundsøe, P., Schnopper, H.W., Lewis, R., Hall, C.H., and Borozdin, K. "The Expanded Beam X-ray Optics Calibration Facility at the Daresbury Synchrotron", *Multilayer and Grazing Incidence X-Ray/EUV Optics II*, Proc. SPIE, Vol. 2011, July 1993.

[11] Dewey, D. *MIT Center for Space Research, HETG Fabrication/Test Memorandum: HX100–HX107, Grating batch JP 12/30/92.* April 5, 1993.

[12] Gmür, Nicholas F., Ed. *National Synchrotron Light Source User's Manual.* February 1991.

[13] Henke, B.L., Gullikson, E.M., and Davis, J.C. "X-ray Interactions: Photoabsorption, Scattering, Transmission, and Reflection at E = 50–30,000 eV, Z = 1–92", *Atomic Data and Nuclear Data Tables*, Vol. 54, July 1993.

[14] Hughes, I.S. *Elementary Particles.* Cambridge: Cambridge University Press, 1991.

[15] Kunz, C., Ed. *Synchrotron Radiation Techniques and Applications.* Germany: Springer-Verlag, 1979.

[16] McKenzie, D.L., Landecker, P.B., Broussard, R.M., Rugge, H.R., Young, R.M., Feldman, U., and Doschek, G.A. "Solar Flare X-ray Spectra between 7.8 and 23.0 Angstroms", *The Astrophysical Journal*, Vol. 241, No. 1, Part 1, October 1, 1980.

[17] Paerels, F.B.S., Bleeker, J.A.M., Brinkman, A.C., Gronenschild, E.H.B.M., and Heise, J. "The High-resolution Soft X-ray Spectrum of HZ 43", *Astrophysical Journal*, Vol. 308, 1986.

[18] Paerels, F.B.S., Bleeker, J.A.M., Brinkman, A.C., and Heise, J. "The High-resolution Photospheric Soft X-ray Spectrum of Sirius B", *Astrophysical Journal*, Vol. 329, 1988.

[19] Schattenburg, Mark. *A Poor Man's Theory of Transmission Diffraction Gratings*, 1982.

[20] Schattenburg, M.L., Canizares, C.R., Levine, A.M., Markert, T.H., and Smith, H.I. "Transmission Grating Spectroscopy and the Advanced X-Ray Astrophysics Facility (AXAF)", *X-Ray Instrumentation in Astronomy II*, Proc. SPIE, Vol. 982, 1988.

[21] Vaiana, G.S., Reidy, W.P., Zehnpfennig, T., VanSpeybroeck, L., and Giaconni, R. "X-ray Structures of the Sun during the Importance 1N Flare of 8 June 1968", *Science*, Vol. 161, 1968.